Borrower: PMC

Lending String: *PBU,IPC,EEM,NHM,SNN

Patron: Borek, Helen

Journal Title: Journal of experimental psychology. Learning, memory, and cognition

Volume: 8 **Issue:** 3
Month/Year: May 1982 **Pages:** 237-242

Article Author:

Article Title: ; Jones, William P.; Anderson, John R. 'Semantic categorization and high-speed scanning.'

Imprint: [Washington, D.C.] ; American Psychologi

ILL Number: 5709520

5709520

Call #:

Location:

ARIEL
Charge
Maxcost: $35.00IFM

Shipping Address:
Hunt Library ILL
Carnegie Mellon University
Frew Street
Pittsburgh, PA 15213-3890
IDS# 187
Fax:
Ariel: 128.2.30.167

9/15

-t, W. N. Formal intralist similarity in pa
ate learning. *Journal of Experimental P*
gy, 1968, *78*, 634–641.
-t, W. N. Ordinal position of letter iden
g stimuli in paired associate learning. *Jour*
perimental Psychology, 1971, *87*, 270–273.
-t, W. N. Stimulus coding and intralist in
e. *Journal of Experimental Psychology*, 197
3–377. (b)
it, W. N. Differences in coding processes
ble for interference. *Journal of Experimen*
ology, 1973, *98*, 404–412.
t, W. N. The assessment of discriminative c
g in paired associate learning. *Memory & Co*
, 1974, *2*, 472–478.
it, W. N. Interference among memory trace
ry & Cognition, 1975, *3*, 143–159. (a)
-t, W. N. Stimulus structure, discrimination, a
erence. *Journal of Experimental Psycholo*
104, 491–500. (b)
t, W. N., & Runquist, P. A. Interference re
n with conceptually similar paired associate
al of Experimental Psychology: Human Lear
nd Memory, 1978, *4*, 370–381.
-t, W. N., & Sekulich, C. Transfer of stimul
ntiation and perceptual selection rules. *Journ*
perimental Psychology: Human Learning a
ry, 1979, *5*, 326–336.
E., & Thomson, D. M. Encoding specific
etrieval processes in episodic memory. *Psych*
l Review, 1973, *80*, 352–373.
E., & Wiseman, S. Relation between reco
and recognition failure of recallable words
in of the Psychonomic Society, 1975, *6*, 79–82.
od, B. J. Attributes of memory. *Psychological*
, 1969, *76*, 559–578.
od, B. J. The role of association in recognition
y. *Journal of Experimental Psychology*, 1974,
17–939.

Received October 28, 1980
Revision received November 5, 1981

Journal of Experimental Psychology:
Learning, Memory, and Cognition
1982, Vol. 8, No. 3, 237–242

0278-7393/82/0803-0237$00.75

Notes, Comments, and New Findings

Semantic Categorization and High-Speed Scanning

William P. Jones and John R. Anderson
Carnegie-Mellon University

Two experiments used versions of Sternberg's item-recognition task, in which the subject could make a decision by semantic categorization or by a search of short-term memory. When a single category distinguished the words of a memory set from foils, pronounced deviations from a linear set-size effect were observed. Decision times were affected little by increases in set size beyond three or four, suggesting that a categorization process was circumventing an item-by-item search of memory. These results were observed in the absence of a consistent mapping between stimuli and responses; in other words, within a session the relevant category constantly changed and stimulus words were used as both targets and foils. The results are compatible with a race model in which memory scanning and semantic categorization occur in parallel; the decision time is determined by the process reaching completion first.

Sternberg (1966) reported that a decision based on a search of memory produced decision times that increased linearly with the number of items to be searched. For small memory loads, this *set-size effect* has proven remarkably robust across a variety of item types, including letters (Nickerson, 1966), digits (Sternberg, 1966), words (Smith, 1967), and random forms (Sternberg, 1969). Sternberg concluded that subjects serially scan through the items of short-term memory (STM).

Experiments demonstrating this linear set-size effect use an *item-recognition paradigm*. In this paradigm, the subject commits a small set of items (usually six or fewer) to memory and must then make a speeded yes/no response regarding the presence or absence of a test item in this set. Targets and foils are commonly all of the same item type, and no feature reliably distinguishes them. In the absence of such a feature, subjects are forced to base their decision on a search of STM.

In experiments in which one or more features do distinguish targets and foils, there is often a substantially reduced and sometimes curvilinear relationship between decision time and set size. This effect was observed by Ellis and Chase (1971) at the perceptual level when foil letters were distinguished from targets by the features of size or color. A letter/digit categorical distinction has been used to similar advantage in the item-recognition task (Lively & Sanford, 1972; Simpson, 1972). In an extension of the item-recognition task, Schneider and Shiffrin (1977) observed almost no effect for set size when targets and foils were separated by the letter/digit distinction. Semantic categorical membership can also apparently facilitate the rejection of foil words (Okada & Burrows, 1973; Reynolds & Goldstein, 1974).

These experiments suggest that decisions are sometimes made on the basis of a categorization process that is relatively unaffected by set size. Such a process would be increasingly likely to be completed before an item-by-item search as set size increases, resulting in the often observed curvilinear relationship between decision time and set size. However, the design in each of the abovementioned experiments creates a form of *response consistency*. In all of these experiments, for example, a proportion of the foils are drawn from a categorically defined set and are never used as targets. Schneider and Shiffrin (1977) argued that response consistency permits the development of an *automatic detection response* that is unaffected by set size. The development of automatic detection is speeded by a target/foil distinction but does not depend on it.

The present study investigated the effects of semantic target/foil distinctions in the absence of response consistency. A central question con-

Preparation of this article was supported by National Science Foundation Grant BNS78-17463. We are grateful to Ann Beattie, Renee Elio, Lynne Reder, and Miriam Schustack for their advice and comments on earlier drafts.

Requests for reprints should be sent to William P. Jones, Department of Psychology, Carnegie-Mellon University, Pittsburgh, Pennsylvania 15213.

Table 1
Stimulus Words for Experiments 1 and 2

HOUR	HORSE	BLUE	HEAD	SHIRT	PIANO
SECOND	LION	GREEN	FINGER	PANTS	DRUM
YEAR	RABBIT	YELLOW	NOSE	BLOUSE	VIOLIN
MINUTE	DEER	PURPLE	TOOTH	COAT	FLUTE
DECADE	SHEEP	WHITE	KNEE	DRESS	GUITAR
WEEK	BEAR	PINK	ANKLE	JACKET	TUBA

cerned the extent to which a categorization process could replace the scanning process as a basis for decisions. Given the speeds with which scanning can take place (much less than 1 sec for sets of fewer than six words), such a replacement would demonstrate a very rapid encoding and utilization of semantic information.

Experiment 1

Method

Materials and design. Memory sets, targets, and foils were all drawn from a stimulus set consisting of six exemplars from each of six categories: units of time, four-legged animals, colors, parts of the human body, articles of clothing, and musical instruments (see Table 1). The words were the most common members of their respective categories, as determined by the Battig and Montague (1969) word norms with the following restrictions: (a) Each word was three to eight letters in length. (b) No more than two words of a category began with the same letter. (c) No word belonged to more than one category of the Battig and Montague norms (e.g., orange). (d) No pairs of words were graphemically or phonemically confusable (e.g., mouth and mouse).

A usable target/foil distinction was established through a manipulation of memory-set type. For sets of multicategory set type, each item represented a different category; in single-category sets all items came from the same category. The factors of set size, test period, and response type were crossed with the factor of set type in a within-subjects design. The size of a memory set ranged from one to six words; an experimental session consisted of six test periods. Within a test period, each of 12 memory sets was tested in a block of 6 targets and 6 foils. The 12 memory sets represented each combination of set size by set type. Each single-category set was randomly selected such that no two sets of a test period came from the same category. Multicategory sets were similarly selected so that no group of words occurred in more than one set.

Within a test block, each of three foils was presented twice. The number of presentations for a memory-set item was in proportion to the set size (approximately, six divided by the set size). Each foil in a test block came from a different category; for single-category sets, none of these categories matched the category of the memory set. Each stimulus word had an equal chance of appearing in any combination of set type by response type within a test period. In an experimental session a word's use as a foil always roughly equalled its use as a target.

Apparatus. The experiment was run on a PDP 11/34 computer using the RSX-11M system. All stimuli were displayed in uppercase letters on a Beehive 100 terminal using a 5 × 7 (per character) dot matrix. The terminal was modified to display stimuli only at the beginning of a video frame; all stimulus-dependent timing was initiated at the beginning of a frame. Yes/no responses were made through a hand-held, two-button box. The left button was labeled "no" and the right button was labeled "yes."

Subjects and procedure. Seven male and six female subjects between the ages of 18 and 26 participated in a single 2-hr. session and were paid between $5 and $8 for their participation. A game format was used in which subjects were awarded points for fast errorless performance; these points were converted into money at the end of the experimental session. Subjects earned a half point for each decision time faster than a "time to beat" (discussed later), and subjects lost two points for each error.

The subjects became familiar with the words and categories through three initial tasks. In an old/new recognition task, each word of the stimulus array was presented twice in a random order and subjects made the appropriate speeded response. In a spelling task, each word was presented for 1 sec, after which the subjects were required to correctly spell the word. A spelling mistake initiated an immediate re-presentation of the word. In an STM span task, the six exemplars of a category were presented, in succession, at 1-sec intervals, and the subject attempted to recall the words in any order. Less than perfect recall brought about an immediate re-presentation of the exemplars in a new order. Each category was tested to a criterion of one perfect recall. After the examplars of the category were correctly recalled in this manner the subjects were prompted to type in a name for the category.

The instructions preceding the item-recognition task (a) informed subjects that a categorical distinction between targets and foils would sometimes exist, and (b) encouraged them to make use of this distinction. Two practice test blocks initiated each test period. These blocks gave a subject the opportunity to win bonus points, and the subject's average decision time for these blocks determined the initial time to beat. Before each of the remaining test blocks in a period, the time to beat was set equal to the smaller of two numbers: (a) the previous time to beat multiplied by 105 msec, or (b) the average of the previous time to beat and the actual mean decision time for the previous block. This number was then adjusted for variations in set size by adding the factor (set size − 3) × 25 msec.

Each test block began with a screen display of (a) the memory set presented in a randomly ordered column, and (b) the time to beat. Subjects viewed the display for as long as they wished. A press of the "return" button on the terminal keyboard terminated the display and initiated a randomly ordered presentation of the test items. Preceding the display of each test item, the word READY appeared on the screen, followed by a 500-msec delay. The screen then cleared, a test item appeared, and the timer began. A press of the yes or no response button terminated the display and stopped the timer. At the end of a test block, subjects were informed of their average decision time, the number of times they were faster than the time to beat, their error rate, their points earned, and their new point total.

Within a test period, memory sets were presented randomly with respect to set size and set type. After every other test period, subjects performed a span task and were then given a 3-min. break. The span task's primary purpose was to break the tedium of the item-recognition task, and span-task results are not reported here.

Results

Decision times and error rates were submitted to an analysis of variance. Decision times were discarded for trials in which an error was made or the time itself exceeded 1 sec. Less than 1% of the correct responses were longer than 1 sec. Figure 1 shows the relationship between performance and set size for the four combinations of set type and response type.

With respect to decision time, main effects in-

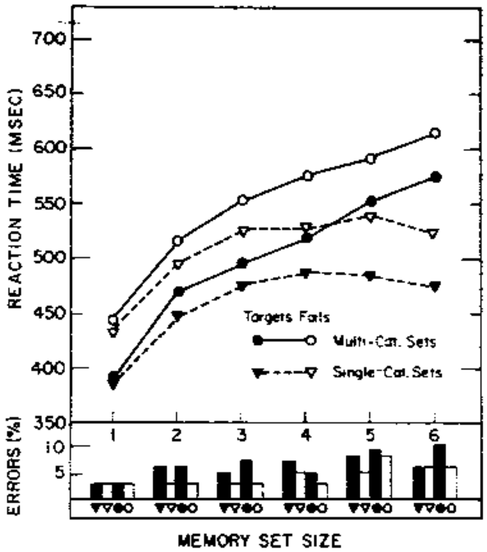

Figure 1. Data from Experiment 1: mean decision times for correct responses and percentages of error as functions of memory-set size (collapsing across test periods).

dicating the advantages of single-category sets, targets, and practice (across test periods) were all significant ($p < .01$). In addition, there was a set-size effect, $F(5, 60) = 114.00$, $p < .001$. However, there was a marked interaction between set size and set type, $F(5, 60) = 22.63$, $p < .001$. The linear component to the relationship between set size and decision time accounts for 92.9% of the variance in the multicategory condition but for only 63.1% of the variance in the single-category condition. In contrast, the quadratic component accounts for 5.6% of the variance in the multicategory condition and for 35.8% of the variance in the single-category condition.

The departure from linearity for the single-category condition can be attributed to an apparent lack of any effect when set size was increased beyond three words. The mean time for a correct yes response in the single-category condition was 473 msec for three-item sets and 475 msec for six-item sets. The mean times for a correct no response were 525 msec and 521 msec for these same two set sizes, respectively.

In the accuracy data, the main effects of set size and response type were both significant ($p < .02$). In agreement with the decision-time results, there was a marginally significant interaction between set size and set type, $F(5, 60) = 1.95$, $p < .10$. There is no indication, then, that the decision-time results can be explained as a simple speed/accuracy trade-off. The overall error rate was 5.3%.

Table 2
Stimulus Words Used to Extend the Stimulus Set for Experiment 2

MONTH	TIGER	BROWN	FOOT	SOCKS	HARP
DAY	MULE	GRAY	LEGS	BELT	TRUMPET
CENTURY	MOUSE	BLACK	ARMS	HAT	BANJO

Discussion

A categorical distinction, in the absence of response consistency, has a clear-cut and dramatic effect on performance in the item-recognition task. The curvilinear relationship between decision time and set size for single-category sets strongly implies a categorization process, which is unaffected by set size.

Ellis and Chase (1971) proposed that categorization at a perceptual level and scanning could take place in parallel, with decision times reflecting the faster to complete of the two processes. In tasks requiring a dual judgment for each item of the memory set, Burrows and Okada (1973, 1976) and Palef (1977) found evidence that semantic information can also be retrieved in parallel with a serial scan.

Categorization and scanning, however, need not take place in parallel to account for the data. Another possible model uses a probabilistic mixture of categorization and scanning (e.g., Atkinson, Herrmann, & Wescourt, 1974). In such a model, the probability that categorization is first attempted for single-category sets of three or more items would have to be near 100% to account for the present results. In fact, subjects in the experiment could have made a strategic commitment to categorization at the beginning of a single-category test block. If they chose to make their decisions on a categorical basis, there would have been no need to even maintain the individual set items in memory, since categorization alone would always have provided the correct response.

The second experiment made such an a priori commitment to categorization impossible. The experiment tested single-category sets in a test block containing an equal number of related foils (same category) and unrelated foils (different categories). Since presentation order for the two foil types was random, the subject would always have to keep the memory set active in order to distinguish targets from related foils. However, it would be possible to reject unrelated foils by means of a category judgment. Of particular interest is the interaction between scanning and categorization in a task where the majority of test items in a block require a serial scan.

Experiment 2

Method

Materials and design. All items of a memory set were drawn from the same semantic category. The factor of foil relatedness replaced the set-type manipulation of Experiment 1. Three foils in a test block were categorically related to the items of the memory set, and the remaining three foils were unrelated. The use of related foils with larger memory sets required an increase in the number of exemplars per category; this was accomplished by adding the words shown in Table 2.

As in the previous experiment, there were six test periods with 12 blocks each. Within a test period, two memory sets of different size were randomly selected from each of the six categories. Three related foils were randomly drawn from the words remaining in a category after a set's selection. The three unrelated foils were randomly drawn from a random collection of three of the five remaining categories. Within an experimental session, each word had an equal chance of appearing as a target and a foil. In addition, each word had an equal chance of appearing as a related and unrelated foil.

Subjects and procedure. Seven male and eight female subjects from the same population used in Experiment 1 participated in a single 2-hr. session and were paid between $5 and $8 for their participation. The familiarization tasks again preceded the item-recognition task. In the span-familiarization task, the word sequence length was reduced from six to five, and each category in Table 2 was tested twice to insure that each word was included in at least one span sequence.

In the instructions preceding the item-recognition task, subjects were encouraged to use category information in the rejection of unrelated foils. In all other respects, experimental procedure and design followed that of Experiment 1.

Results

Figure 2 shows the relationship between performance and set size for the three test-item types (targets, related foils, and unrelated foils). Decision times were screened using the procedure described for Experiment 1. Again, fewer than 1%

riment 2

SOCKS	HARP
BELT	TRUMPET
HAT	BANJO

Experiment 2

als and design. All items of a memory
drawn from the same semantic category.
r of foil relatedness replaced the set-type
tion of Experiment 1. Three foils in a
were categorically related to the items
mory set, and the remaining three foils
lated. The use of related foils with larger
sets required an increase in the number
lars per category; this was accomplished
g the words shown in Table 2.
the previous experiment, there were six
ds with 12 blocks each. Within a test
wo memory sets of different size were
selected from each of the six categories.
lated foils were randomly drawn from the
naining in a category after a set's selec-
three unrelated foils were randomly
om a random collection of three of the
ning categories. Within an experimental
ach word had an equal chance of ap-
s a target and a foil. In addition, each
an equal chance of appearing as a re-
unrelated foil.
ts and procedure. Seven male and eight
bjects from the same population used in
nt 1 participated in a single 2-hr. session
paid between $5 and $8 for their par-
The familiarization tasks again pre-
item-recognition task. In the span-fa-
ion task, the word sequence length was
rom six to five, and each category in
as tested twice to insure that each word
ed in at least one span sequence.
instructions preceding the item-recog-
, subjects were encouraged to use cat-
ormation in the rejection of unrelated
other respects, experimental procedure
n followed that of Experiment 1.

2 shows the relationship between per-
and set size for the three test-item types
elated foils, and unrelated foils). De-
es were screened using the procedure
for Experiment 1. Again, fewer than 1%

of the correct responses exceeded 1 sec. The data for three subjects were excluded from the analysis because of an error rate exceeding 10%. (A separate analysis of the data for these three subjects produced complete agreement with the results from the remaining subjects, which follow.)

An analysis of the decision times revealed significant main effects of practice (across test periods) and set size ($p < .001$). Unrelated foils were rejected significantly faster than related foils were, $F(1, 11) = 130.43$, $p < .001$. The differential effect of set size on the three test-item types is reflected in a significant interaction, $F(10, 110) = 22.97$, $p < .001$. In order to understand this interaction, the two foil conditions were separately considered in relation to targets. The effect of set size was significantly less for unrelated foils than it was for targets, $F(5, 55) = 16.95$, $p < .001$. On the other hand, the effect of set size was significantly greater for related foils than it was for targets, $F(5, 55) = 3.57$, $p < .01$. The linear component of the relationship between set size and decision time accounted for 98.9% of the variance for related foils and 91.7% of the variance for unrelated foils. The quadratic component accounted for less than 1% of the variance for related foils and for 7.9% of the variance for unrelated foils. For targets, the linear component accounted for 92.3% of the variance and the quadratic component accounted for 6.1% of the variance. These figures for targets are in close agreement with the corresponding figures for the multicategory condition of Experiment 1.

In the error data, a main effect for set size was significant, $F(5, 55) = 15.13$, $p < .001$. The decision-time advantage for unrelated over related foils was reflected in error rates as well, $F(1, 11) = 13.24$, $p < .004$. Set size had a significantly greater impact on error rates for related foils than for targets, $F(5, 55) = 5.48$, $p < .001$. There was no significant interaction in the relationship between set size and targets versus unrelated foils ($p > .17$). However, error rates for targets were significantly greater than for unrelated foils, $F(1, 11) = 46.75$, $p < .001$. The error rates for unrelated foils were by far the lowest of the three conditions and were obviously unaffected by increases in set size. There is no indication that decision-time differences are solely the result of a speed/accuracy trade-off.

Discussion

Although most of the trials in a test block required a memory scan, the categorization process continued to facilitate the rejection of unrelated foils, especially at the larger set sizes. The total increase in decision time as set size ranged from four to six was only 15 msec for unrelated foils, in comparison to a 74-msec increase for related foils and a 44-msec increase for targets. The average time to reject an unrelated foil at these larger set sizes is virtually identical to the rejection time for single-category foils in Experiment 1 (528 vs. 529 msec). The greater linearity of the decision-time slope may indicate that decisions for unrelated foils were sometimes based on a serial scan for even the larger set sizes.

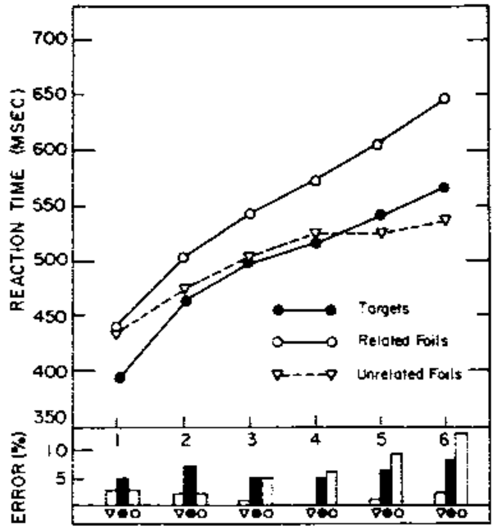

Figure 2. Data from Experiment 2: mean decision times for correct responses and percentages of error as functions of memory-set size (collapsing across test periods).

Both the decision-time and error-rate slopes are significantly steeper for related foils than for targets,[1] suggesting that the category membership of a foil may impede as well as facilitate its rejection. This is further indicated by a comparison of Experiments 1 and 2, in which differences in performance are noticeable for sets of five and six items. For these set sizes, targets in Experiment 2 are about 12 msec faster than multicategory targets in Experiment 1. In contrast, related foils in Experiment 2 are about 24 msec slower than multicategory foils in Experiment 1. In addition,

[1] If the decision-time slope for related foils is depressed as a result of a speed/accuracy trade-off (a possibility suggested by the high error rates for related foils), then the slope may actually be in a 2:1 relationship with the decision-time slope for targets. Therefore, subjects may have used a terminating search to distinguish targets from related foils. However, it is not clear why a terminating search would selectively produce such high error rates for related foils.

error rates are considerably higher for related foils at the larger set sizes. Poor performance for related foils could occur in a parallel model as the result of a response competition between the categorization process and scanning. It is likely that a suppression of the category yes response would take extra time; a failure to suppress this response would lead to an error.

General Discussion

The results of these two experiments are perhaps best described in terms of a parallel race model involving serial scanning and the categorization process. Categorization dominated for sets of more than three or four items and was unaffected by changes in set size. These effects were observed in the absence of a consistent mapping between stimuli and responses. In both experiments the relevant category changed after every 12 trials, and stimulus words were used equally often as targets and foils.

The results demonstrate a use of semantic information to circumvent an item-by-item search of memory. Similar results have been obtained in the fact-retrieval paradigm of long-term memory (McCloskey & Bigler, 1980; Reder & Anderson, 1980; Smith, Adams, & Schorr, 1978). In the experiments of Reder and Anderson, for example, interference did not occur among a set of thematically related facts when foils were thematically unrelated. Interference returned, however, when thematically related foils were used.

References

Atkinson, R. C., Herrmann, D. J., & Wescourt, K. T. Search processes in recognition memory. In R. L. Solso (Ed.), *Theories in cognitive psychology: The Loyola Symposium.* New York: Wiley, 1974.

Battig, W. F., & Montague, W. E. Category norms for verbal items in 56 categories: A replication and extension of the Connecticut category norms. *Journal of Experimental Psychology Monograph*, 1969, *80*(3, Pt. 2).

Burrows, D., & Okada, R. Parallel scanning of semantic and formal information. *Journal of Experimental Psychology*, 1973, *97*, 254–257.

Burrows, D., & Okada, R. Parallel scanning of physical and category information. *Memory & Cognition*, 1976, *4*, 31–35.

Ellis, S. H., & Chase, W. G. Parallel processing in item recognition. *Perception & Psychophysics*, 1971, *10*, 379–384.

Lively, B. L., & Sanford, B. J. The use of category information in a memory search task. *Journal of Experimental Psychology*, 1972, *93*, 379–385.

McCloskey, M., & Bigler, K. Focused memory search in fact retrieval. *Memory & Cognition*, 1980, *8*, 253–264.

Nickerson, R. S. Response times with a memory-dependent decision task. *Journal of Experimental Psychology*, 1966, *72*, 761–769.

Okada, R., & Burrows, D. Organizational factors in high-speed scanning. *Journal of Experimental Psychology*, 1973, *101*, 77–81.

Palef, S. R. Searching memory for physical and semantic information. *Canadian Journal of Psychology*, 1977, *31*, 131–138.

Reder, L. M., & Anderson, J. R. A partial resolution of the paradox of interference: The role of integrating knowledge. *Cognitive Psychology*, 1980, *12*, 447–472.

Reynolds, J. H., & Goldstein, J. A. The effects of category membership on memory scanning for words. *American Journal of Psychology*, 1974, *87*, 487–495.

Schneider, W., & Shiffrin, R. M. Controlled and automatic human information processing: I. Detection, search and attention. *Psychological Review*, 1977, *84*, 1–66.

Simpson, P. J. High-speed memory scanning: Stability and generality. *Journal of Experimental Psychology*, 1972, *96*, 239–246.

Smith, E. E. Effects of familiarity on stimulus recognition and categorization. *Journal of Experimental Psychology*, 1967, *74*, 324–332.

Smith, E. E., Adams, N., & Schorr, D. Fact retrieval and the paradox of interference. *Cognitive Psychology*, 1978, *10*, 438–464.

Sternberg, S. High-speed scanning in human memory. *Science*, 1966, *153*, 652–654.

Sternberg, S. Memory scanning: Mental processes revealed by reaction-time experiments. *American Scientist*, 1969, *57*, 421–457.

Received February 24, 1981
Revision received October 8, 1981 ■

Journal of Experimental Psychology:
Learning, Memory, and Cognition
1982, Vol. 8, No. 3, 243–251

Strategic

A

Adult subjects' strategies in t
were studied in three experim
of either an array rotating rel
rotating relative to a fixed a
logically equivalent problems
lems differed in overall difficu
terns. The data suggested that
problems. For viewer rotation
a more abstract frame of refer
only one element at a time.
functional "unit" of spatial tr

In the past decade there has been a tre
growth of interest in the processes involve
tial reasoning. Much of this interest has
from studies of the "mental rotation" p
non by Shepard and his colleagues (e.g.
& Shepard, 1973; Metzler & Shepar
Shepard, 1975; Shepard & Metzler, 19
variety of related tasks, chronometric d
supported a powerful process model of ho
abstractly manipulate spatial informatio
tasks have generally dealt with figures p
chistoscopically, and the mental rotatio
proposes that adults holistically rotate
res in an analog fashion.

In the current experiments, adult spa
oning was examined across a wider rang
demands than has typically been studi
logically equivalent spatial reasoning p
were compared using object arrays and
questioning procedures. In the first type
lem (directly akin to those studied by S
subjects predicted the outcome of a rota
array relative to a stationary viewer (
tation problem). In the second problem
predicted the outcome of a rotation of
around the periphery of a stationary array
rotation problem).

These array-rotation and viewer-rotat
lems were contrasted for three types of
ng procedure that probed different aspe
ransformed spatial information. The th
on types were termed appearance, item

The author thanks Sue Somerville, Don H
ecially Laurie Chassin and Linda Smith
mments on earlier drafts of this article.

Requests for reprints should be sent to Cla
, Department of Psychology, Arizona Sta
y, Tempe, Arizona 85281.

Chemical Geology, 88 (1990) 223–243
Elsevier Science Publishers B.V., Amsterdam

[5]

Interaction between water and melt in the system $CaAl_2O_4$–SiO_2–H_2O

Bjørn O. Mysen
Geophysical Laboratory, 5251 Broad Branch Rd., N.W., Washington, DC 20015 (U.S.A.)

(Received November 7, 1989; revised and accepted May 15, 1990)

ABSTRACT

Mysen, B.O., 1990. Interaction between water and melt in the system $CaAl_2O_4$–SiO_2–H_2O. Chem. Geol., 88: 223–243.

The interaction between dissolved H_2O and melt structure on the join $CaAl_2O_4$–SiO_2–H_2O has been studied with Raman spectroscopy. The total H_2O contents ranged from 3 to 10 wt.% with Al/(Al+Si) = 0–0.333. The spectra are consistent with formation of OH complexes that include all Ca^{2+} and Al^{3+} in addition to molecular H_2O. No direct evidence for (Si,Al)–OH bonds can be discerned in the spectra of hydrous calcium aluminosilicate melt (the 970-cm^{-1} band from Si–OH stretching observed in the spectra of SiO_2–H_2O melts is not well resolved in aluminous samples). However, the spectral topology of the fundamental OH stretch bands near 3600 cm^{-1} can only be rationalized if some Si–OH or (Si,Al)–OH bonding exists in the melts.

The melts become depolymerized as H_2O is dissolved to form Ca..OH and Al..OH complexes. Formation of Ca..OH complexes is a more efficient depolymerization mechanism than that of Al..OH complexes [6 vs. $\frac{3}{4}$ nonbridging oxygen would be formed per mole H_2O dissolved as a Ca..OH complex of $Ca(OH)_2$ type vs. an Al..OH complex of $Al(OH)_3$ type]. With increasing Al/(Al+Si) of the melts complexing of OH with Al^{3+} (Al..OH) probably becomes more important at the expense of complexes with Ca^{2+} (Ca..OH). Thus, the effect of dissolved H_2O on melt polymerization diminishes with Al/(Al+Si). However, the degree of polymerization of the melts (NBO/T) for a given total H_2O concentration is less than that expected by either the Ca..OH or the Al..OH complexing mechanism alone. The excess water is present as molecular H_2O and as (Si,Al)–OH bonds that replace (Si,Al)–O–(Si,Al) bridging oxygen bonds in the melts.

1. Introduction

Dissolved water affects chemical and physical properties of silicate melts. For example, transport properties are strongly enhanced in hydrous melts compared with their anhydrous equivalents. Melt viscosity can be lowered by up to several orders of magnitude (e.g., Shaw, 1963; Kushiro, 1978; Dingwell and Mysen, 1985). Cation diffusivity is increased (Watson, 1979) as is electrical conductivity (Takata et al., 1981; Satherley and Smedley, 1985). Liquidus relations are also significantly affected by water, generally resulting in a decrease in silica activity (e.g., Kushiro et al., 1968; Kushiro, 1972, 1989; Mysen and Boettcher, 1975; Carmichael et al., 1976).

The relationships between melt properties and water activity together with P–V–T measurements of hydrous $NaAlSi_3O_8$ composition melt have have led to inference that the melts become depolymerized upon solution of H_2O through the replacement of bridging oxygen with OH groups and an exchange of H^+ from H_2O with Na^+ in the melt (Uys and King, 1963; Burnham, 1974, 1975). However, water solubility data for alkali aluminosilicate systems (Oxtoby and Hamilton, 1978; Hamilton and Oxtoby, 1986) are suggestive of multiple OH species. From spectroscopic studies in the Na_2O–Al_2O_3–SiO_2 system, a variety of metal–OH bonding types in silicate melts have been inferred (Mysen and Virgo, 1986a). In addition, molecular H_2O can be important in sili-

009-2541/90/$03.50

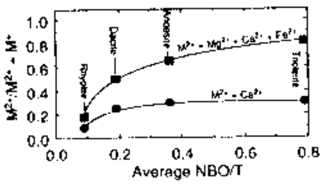

Fig. 1. Proportion of divalent metal cations (M^{2+}) relative to monovalent and divalent metal cations in common natural magmatic liquids as a function of their degree of polymerization (NBO/T). Chemical analyses from Chayes (1975a, b, and unpublished data, 1985). Calculation of NBO/T as described by Mysen (1988).

cate melts (e.g., Hodges, 1974; Epel'baum et al., 1975; Persikov, 1975; Stolper, 1982; Eggler and Burnham, 1984; Epel'baum, 1985; Navrotsky, 1987; Silver and Stolper, 1989). However, the relative abundance of molecular H_2O and OH groups remains a matter of discussion (e.g., Dingwell and Webb, 1989a, b; Silver and Stolper, 1989).

A common feature of the majority of studies on solubility and solubility mechanisms of H_2O in silicate melts is that the base compositions were alkali aluminosilicates, commonly on the join $NaAlO_2$–SiO_2. Data in this system are fundamentally important for characterization of the role of water in magmatic liquids, but alkali metals in general (K^+ and Na^+) and Na^+ in particular, are not the principal cations in magmatic liquids (Fig. 1). With the exception of rhyolite, ≥50% of the metal cations in common magmatic liquids are divalent (Ca^{2+}, Mg^{2+} and Fe^{2+}). Over 50% of the divalent cations are represented by Ca^{2+} (Mysen, 1988). From these simple observations, it is evident that in order to understand the interaction between water and natural magmatic liquids, experimental data for alkaline-earth aluminosilicate melts are needed. As a step in this direction, interactions between H_2O and melts in the system CaO–Al_2O_3–SiO_2 have been examined.

2. Experimental methods

Starting materials were glasses formed by melting $CaCO_3+Al_2O_3+SiO_2$ oxide mixtures at 1550–1660°C for 1–4 hr. subsequent to decarbonation of $CaCO_3$ at ~1300°C in vertical quench furnaces. Detailed chemical characterization of these materials were given in Seifert et al. (1982). All compositions, CA2*S14*, CA2*S8*, CA2*S6* and CA2*S4*, are on the join $CaAl_2O_4$–SiO_2 with their Al/(Al+Si)=0.125, 0.200, 0.25 and 0.333 for the compositions CA2*S14*, CA2*S8*, CA2*S6* and CA2*S4*, respectively. The SiO_2 starting material was the same commercial silica glass also used by Hemley et al. (1986) and Mysen and Virgo (1986a). The water was double-distilled and deionized before use, and D_2O was 95.7% D_2O with the remainder as light water. The water was loaded into Pt capsules with a microsyringe with a ±0.05 μl precision. The uncertainty of the water concentration in the sample from the combined weighting errors is < ±5%. The H_2O contents ranged from 3 to 10 wt.%, which are less than the water solubility in these melt compositions under the pressure and temperature conditions of synthesis (McMillan et al., 1986).

The hydrous glasses were produced in the solid-media, high-pressure apparatus (Boyd and England, 1960). About 20-mg samples together with known amount of H_2O (or D_2O) in sealed Pt capsules were subjected to 13–15 kbar and 1500–1700°C with run duration ranging from 1.5 to 64 hr. (Table 1) in 0.5-in. (1.27 cm) diameter Pyrex® glass–AlSiMag furnace assemblies without external control of the f_{H_2}. The quenching rates (by turning off the power to the furnace) from experimental conditions with the 0.5-in. (1.27 cm) diameter furnace assemblies in steel pressure plates of 7-in. (17.78 cm) diameter by 2-in. (5.08 cm) thickness (water-cooled above and below) are distinct nonlinear functions of time since quench (Fig. 2). In general, though, the rate is near 100°C s^{-1} from the experimental temperatures between 500° and 600°C (the 100°C s^{-1} rate is shown as dashed lines in Fig. 2).

TABLE 1

Synthesis conditions of high-pressure, hydrous glasses

Run No.	Starting material	Volatile (wt.%) H_2O	Volatile (wt.%) D_2O	Pressure (kbar)	Temperature (°C)	Run duration (hr.)
SiO_2:						
2342	SiO_2	3		15	1,700	1.5
2507	SiO_2	4		13	1,600	8.5
2257	SiO_2	5		15	1,500	64
2271	SiO_2		5	15	1,550	30
2508	SiO_2	7.5		13	1,600	5.5
2299	SiO_2	10		15	1,550	22
CA2*S14*:						
2345	CA2*S14*	3		15	1,600	5
2346	CA2*S14*	5		15	1,600	5
2589	CA2*S14*		5	15	1,550	2
2347	CA2*S14*	10		15	1,600	5
CA2*S8*:						
2348	CA2*S8*	3		15	1,600	5
2349	CA2*S8*	5		15	1,600	5
2607	CA2*S8*		5	15	1,550	4
2350	CA2*S8*	10		15	1,600	5
CA2*S6*:						
2352	CA2*S6*	3		15	1,550	4
2353	CA2*S6*	5		15	1,550	4
2606	CA2*S6*		5	15	1,550	4
2354	CA2*S6*	10		15	1,550	4
CA2*S4*:						
2355	CA2*S4*	3		15	1,550	4
2356	CA2*S4*	5		15	1,550	4

All but the most water-rich samples quench to clear, bubble-free (on an optical microscopic scale) glass. Samples with 10 wt.% H_2O exhibited a tendency to form finely disseminated bubbles that most likely reflect exsolution of water upon quenching. The bubbles (when observed) are likely to be formed upon quenching because the water solubility in these melts exceeds 10 wt.% (the maximum H_2O content of the experimental samples) under the experimental conditions (McMillan et al., 1986).

Structural information was obtained with an

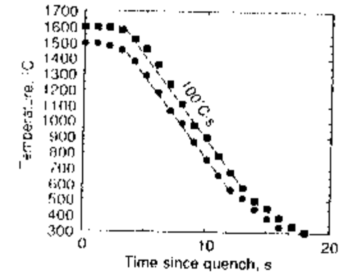

Fig. 2. Quenching rates (expressed as temperature since quench) of solid-media, high-pressure apparatus used in the experiments.

automated Raman spectroscopy system (Mysen et al., 1982) with the 532-nm line of a frequency-doubled Nd-YAG laser and the 480-nm line of an Ar^+ laser for sample excitation. In both cases, the samples were excited with ~0.5 W at the ~1-mm^3 samples.

The spectra were recorded in two segments. The lower-frequency segment (300–1800 cm^{-1}) includes the range of (Si,Al)–O and (Si,Al)–OH vibrations, and the 1600-cm^{-1} region of possible H–O–H bending. The higher-frequency segment (3000–4000 cm^{-1}) includes the range of OH stretch vibrations. For deuterated samples, the latter region is 2000–3000 cm^{-1}.

In order to maximize the amount of structural information that could be obtained, the spectra were curve-fitted statistically (Mysen et al., 1982). The background was subtracted from the uncorrected spectra by least-squares fitting of a line through the data points at frequencies where Raman scattering was observed. Prior to statistical analysis, the spectra were corrected for temperature- and frequency-dependent scattering intensity (e.g., Long, 1977). The Raman intensities in each fitted spectrum were normalized to the data point of the greatest absolute intensity. The curve-fitting (Seifert et al., 1981, 1982; Mysen et al., 1982) was carried out statistically with the method of minimization of least squares

(Fletcher and Powell, 1963; D
Upon convergence, the minim
and maximum randomness in
bution are obtained. All line p
quency, half-width and intensit
number of lines were independ
the fitting routine.

Several important aspects
interpretations rely on system
the curve-fitted spectra. Some
are not always visually evident
desirable to ascertain the relia
ting procedure in some detail
ument that the best fit has bee
necessary to address (1) whe
chosen line-shape is appropria
for a given fit the χ^2-minimum
convergence is global or reg
whether the number of lines i
in fact the number that leads t
χ^2 and maximum randomness
These factors have been addre
anhydrous, depolymerized me
minosilicate systems (Mysen,
was concluded that the resul
routine fulfill these requiremen
a successful comparison of s
mation with data obtained b
netic resonance (NMR) spec
further to our confidence in th
analysis.

Similar procedures were em
fitting spectra of the hydrous
nosilicate glasses. From thes
dures it was found that the sp
$CaAl_2O_4$–SiO_2–H_2O quenche
fitted with symmetric Gauss
commonly the case for Ra
amorphous materials (e.g.,
Hartwig, 1977; Seifert et a
McMillan et al., 1982; Mys
McKeown et al., 1984; Mysen,
or not the minima in χ^2 are r
is not easily subjected to rig
tests. However, for each fitte
input trial parameters were ran

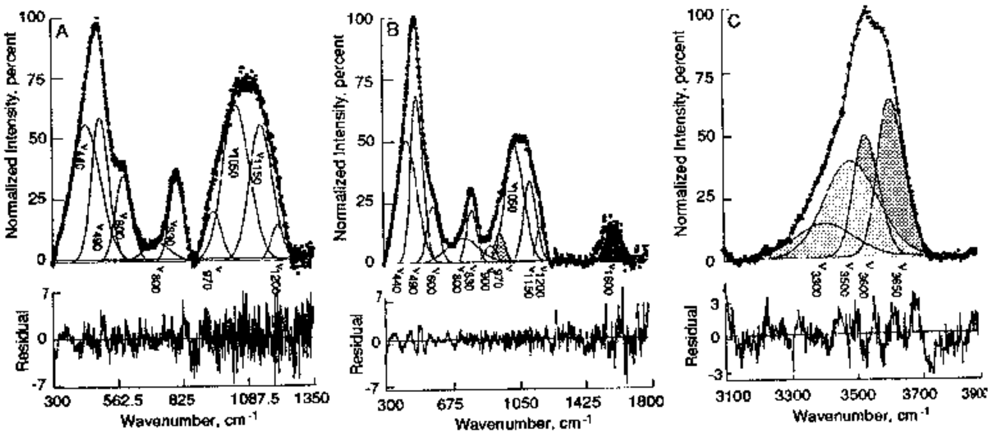

Fig. 4. Examples of Raman spectra of (A) anhydrous CA2S8; (B) low-frequency segment of CA2S8 + 5 wt.% H_2O; (C) and high-frequency envelope of CA2S8 + 5 wt.% H_2O.

alkaline-earth aluminate–silica melt, the proportion of the two structural types changed, but not the Al/(Al+Si) of the individual units (Fig. 5). This structural interpretation by anhydrous $CaAl_2O_4$–SiO_2 melt structure differs from that for $NaAlO_2$–SiO_2 melts where Al/(Al+Si) of the individual three-dimensional structural units is positively correlated with the bulk melt Al/(Al+Si).

The low-frequency region (300–1800 cm^{-1}) of the spectra of hydrous samples can be divided into three distinct segments (Figs. 3 and 4). In the region from 300 to ~600 cm^{-1} all spectra show an envelope with a peak maximum near 500 cm^{-1}. This envelope has a small shoulder on its high-frequency limb (~600 cm^{-1}). There is a higher-frequency segment between ~800 and ~1300 cm^{-1} consisting of a distinctive band or two bands near 800 cm^{-1} and a group of three of five bands in the envelope between 900 and 1300 cm^{-1}. Finally, all the hydrous samples show a distinct band near 1600 cm^{-1}. Those of anhydrous materials do not.

For all compositions, the envelope centered near 500 cm^{-1} sharpens as H_2O is dissolved in the material. Three bands have been fitted to this envelope (ν_{440}, ν_{490} and ν_{600}; see Figs. 3A, B and 4A, B). The central band near 490 cm^{-1} is more dominant in the spectra of hydrous materials than in the anhydrous equivalent. Furthermore, in spectra of the hydrous samples, the ν_{600} band is less intense relative to the rest of this frequency region (Fig. 6). This behaviour of the 600-cm^{-1} band, first noted by Stolen and Walrafen (1976) for SiO_2–H_2O glass, is similar to that for melts in the system $NaAlO_2$–SiO_2 (Mysen and Virgo, 1986a).

Solution of H_2O in calcium aluminate–silica melts results in several changes in the high-frequency portion of the Raman spectra (Figs. 3 and 4). The frequencies of all the bands in the 900–1300-cm^{-1} region show a continuous decrease with increasing Al/(Al+Si) (Fig. 7). In the spectra of SiO_2–H_2O melts a narrow band appears near 970 cm^{-1} (Fig. 3). With D_2O in replacement for H_2O this band shifts to ~950 cm^{-1} (Table II). The band is slightly asymmetric, and Mysen and Virgo (1986a) suggested that two Gaussian lines with different line-width should be fitted to this peak in order to satisfy the spectral signal. The frequency of the band or two bands near 970 cm^{-1} SiO_2–H_2O melts is insensitive to water content. Its

TABLE II

Frequencies of Raman bands in the 300–1800-cm^{-1} range

Al/(Al+Si)	440	490	600	650	800	830	900	970	1,050	1,150	1,200	1,600
Anhydrous:												
0	449±1	495±1	608±1		800±1	840±1			1,062±1	1,161±1	1,213±1	
0.125	453±1	492±1	595±1		735±1	805±1		952±1	1,069±1	1,125±1	1,189±1	
0.2	440±1	497±1	591±1		724±1	803±1		954±1	1,047±1	1,145±1	1,209±1	
0.25	449±1	505±1	586±1		713±1	802±1		939±1	1,018±1	1,123±1	1,197±1	
0.333	437±1	495±1	590±1			787±1		930±1	996±1	1,100±1		
3 wt.% H_2O:												
0	439±1	484±1	589±1		788±1	822±1		968±1	1,060±1	1,194±1	1,239±1	1,621±1
0.125	427±1	490±1	583±1		728±3	806±1	914±2	967±1	1,050±1	1,167±1	1,167±1	1,627±1
0.2	409±1	499±1	610±1		718±4	821±1	926±5	999±2	1,080±2	1,215±3	1,215±3	1,665±2
0.25	436±2	516±1	602±3	650±5	766±4	816±2	889±2	924±4	1,148±5	1,207±3	1,207±3	1,605±2
0.333	461±1	508±1	594±1		728±1	797±1	871±1		1,009±1	1,180±1	1,180±1	1,618±1
4 wt.% H_2O:												
0	443±1	480±1	577±2		791±1	826±1		961±1	1,066±1	1,164±2	1,221±2	1,608±1
5 wt.% H_2O:												
0	443±1	483±1	570±1		788±1	821±1		963±1	1,063±1	1,167±1	1,211±1	1,615±1
0.125	449±1	477±1	596±1		712±1	803±1	902±2	964±2	1,052±2	1,156±2	1,197±1	1,635±1
0.2	436±1	494±1	581±1		748±2	801±1	906±2	958±1	1,046±1	1,133±1	1,191±1	1,589±1
0.25	440±1	500±1	587±1		742±1	793±1		908±1	1,037±1	1,132±1	1,190±1	1,630±1
0.333	454±1	523±1	609±1		725±1	800±1	890±1		0,019±2	1,120±1	1,188±1	1,637±1
7.5 wt.% H_2O:												
0	447±1	484±1	578±1		788±1	810±1		962±1	1,062±1	1,163±1	1,212±1	1,633±1
10 wt.% H_2O:												
0	445±1	484±1	572±1		792±1	825±1		964±1	1,064±1	1,168±2	1,215±1	1,623±1
0.125	449±1	490±1	594±1		748±1	807±1	882±1	964±1	1,045±1	1,131±1	1,200±1	1,629±1
0.2	456±2	494±1	586±1		753±2	798±2	889±1	942±1	1,046±1	1,140±1	1,194±1	1,630±1
0.25	462±1	497±1	585±1		696±2	787±1	874±1	909±1	1,056±1	1,123±1	1,181±1	1,634±1
5 wt.% D_2O:												
0	447±1	484±1	594±1		793±1	827±1		948±1	1,065±1	1,174±1	1,217±1	
0.125	448±1	504±1	593±1		747±1	820±1	905±1	960±1	1,062±1	1,150±1	1,219±1	
0.2	461±1	510±1	599±1		747±2	819±2	900±1	952±2	1,067±5	1,160±4	1,219±2	
0.25	481±1	516±1	598±1		720±1	793±1	879±1	906±1	1,006±1	1,087±1	1,105±1	

intensity may increase in the water concentration range between 3 and 5 wt.%, and also increases slightly relative to that of the 1600-cm^{-1} band in this water concentration range. Higher water contents (> 7.5 wt.%) may cause this intensity ratio, $A_{970}/(A_{970}+A_{1600})$, to decrease (see also further discussion on pp. 233–234).

The appearance of the 1600-cm^{-1} band in spectra of Al-bearing melts on the $CaAl_2O_4$–SiO_2 join band is similar to that of pure SiO_2, and also resembles that of melts on the join

TABLE III

Frequencies in the 3000–4000-cm^{-1} region

Al/(Al+Si)	3,300	3,500	3,600	3,650
3 wt.% H_2O:				
0	3,460±6	3,570±3	3,595±1	3,659±1
0.125	3,273±5	3,473±5	3,576±1	3,654±3
0.2	3,269±1	3,437±1	3,533±1	3,623±1
0.25	3,267±1	3,391±1	3,533±1	3,628±1
0.333	3,338±2	3,454±2	3,587±1	
4 wt.% H_2O:				
0	3,348±1	3,541±1	3,595±1	3,660±1
5 wt.% H_2O:				
0	3,305±1	3,515±1	3,594±1	3,661±1
0.125	3,273±1	3,487±2	3,565±1	3,641±2
0.2	3,412±9	3,498±3	3,546±1	3,623±1
0.25	3,272±4	3,464±2	3,588±1	3,648±1
0.333	3,305±2	3,505±1	3,568±2	3,634±2
7.5 wt.% H_2O:				
0	3,307±1	3,514±1	3,595±1	3,658±1
10 wt.% H_2O:				
0	3,317±2	3,505±1	3,595±1	3,657±1
0.125	3,185±6	3,480±6	3,570±2	3,660±1
0.2	3,282±1	3,427±1	3,559±1	3,633±1
0.25	3,271±9	3,434±4	3,556±1	3,629±1
5 wt.% D_2O:				
0	2,536±1	2,578±4	2,642±2	2,700±1
0.125		2,552±2	2,683±2	2,683±1
0.2	2,205±1	2,501±1	2,621±1	2,692±1
0.25	2,215±3	2,480±3	2,601±1	2,679±1

TABLE IV

Relative areas of Raman bands in the 3000–4000-cm^{-1} range

Al/(Al+Si)	3,300	3,500	3,600	3,650
3 wt.% H_2O:				
0	22.8±1.5	35.8±2.4	12.3±0.8	29.3±1.7
0.125	11.0±1.6	39.7±4.7	36.7±4.3	12.7±1.3
0.2	2.4±01.	20.9±1.1	29.2±0.4	47.5±0.9
0.25	23.0±1.1	4.5±0.4	59.4±1.9	13.3±0.6
0.333		38.0±1.8	59.4±1.7	13.3±0.8
4 wt.% H_2O:				
0	45.0±2.4	29.3±1.4	11.7±0.6	14.1±0.7
5 wt.% H_2O:				
0	42.8±2.5	30.9±1.4	15.9±0.6	10.4±0.6
0.125	5.4±0.8	47.4±2.5	37.5±2.0	13.9±0.6
0.2	13.9±1.5	35.8±7.3	21.4±3.5	28.9±5.9
0.25	19.1±1.5	35.9±2.2	42.9±2.2	2.1±0.2
0.333	27.3±1.6	48.2±1.6	12.7±0.8	11.8±0.8
7.5 wt.% H_2O:				
0	39.3±1.3	44.8±1.3	8.1±0.4	7.9±0.4
10 wt.% H_2O:				
0	55.4±1.7	30.8±1.0	7.6±0.3	6.2±0.3
0.125	11.6±0.7	48.3±2.5	30.4±2.0	9.7±0.8
0.2	19.7±1.1	21.6±0.8	54.8±1.7	3.9±0.3
0.25	24.0±2.2	29.3±1.4	44.7±4.5	2.0±0.2
5 wt.% D_2O:				
0	42.4±3.5	10.7±1.8	25.1±2.4	21.8±1.7
0.125		59.8±4.8	28.4±3.0	12.0±1.3
0.2	8.1±1.2	37.4±2.1	45.5±2.3	9.0±0.6
0.25	4.4±0.9	44.1±2.8	42.5±2.7	9.0±0.6

$NaAlO_2$–SiO_2 (McMillan and Remmele, 1986; Mysen and Virgo, 1986a). The band is assigned to H–O–H bending and requires the presence of molecular H_2O in the sample (Scholze, 1960; Stolper, 1982).

The 970-cm^{-1} band in the spectra of quenched hydrous silica melt is assigned to Si–OH stretching (e.g., Stolen and Walrafen, 1976). The ~15-cm^{-1} frequency reduction by substitution of ^{2}H for ^{1}H is consistent with the anticipated frequency decrease caused by the mass difference of the oscillators (Freund, 1982) in Si–OH and Si–OD (with a theoretical 12-cm^{-1} decrease, see also additional discussion on p. 232). Mysen and Virgo (1986a) suggested that the two bands fitted to the 970-cm^{-1} region of the SiO_2–H_2O spectra could be interpreted as being due to perhaps more than one Si–OH bond in Si–O(OH) tetrahedra in analogy with multiply F for O-substituted SiO_4 tetrahedra in SiO_2 (Yamamoto et al., 1983). This suggestion is not supported by ^{1}H NMR of SiO_2–H_2O glasses (Farnan et al., 1987; Eckert et al., 1988). Whether more than one Si-

TABLE V

Areas of individual bands in the 300–1800-cm^{-1} range relative to total area

Al/(Al+Si)	440	490	600	650	800	830	900	970	1,050	1,150	1,200	1,600
Anhydrous:												
0	46.4±2.6	7.1±0.5	5.0±0.5		11.6±0.8	5.4±0.3	1.0±0.3		9.8±0.7	6.3±0.7	7.1±0.6	
0.125	32.1±2.0	6.7±0.4	5.2±0.4		1.6±0.2	9.2±0.9		3.2±0.2	26.4±2.1	2.9±0.3	13.3±1.0	
0.2	21.1±1.8	13.7±1.0	7.7±0.8		2.7±0.2	6.5±0.5		4.4±0.3	22.8±2.0	22.0±1.9	2.8±0.2	
0.25	12.0±0.7	11.6±0.5	10.8±0.5		6.9±0.5	5.2±0.3		4.3±0.3	22.4±1.1	27.0±1.1	3.7±0.5	
0.333	35.1±2.5	21.8±3.0	4.0±0.5		3.1±0.3			3.0±0.2	12.8±1.0	24.9±1.9		
3 wt.% H_2O:												
0	41.9±4.1	12.1±1.3	1.0±0.3		5.4±0.6	7.3±0.8		15.3±1.7	4.4±0.6	3.3±1.5	7.0±1.1	9.0±1.1
0.125	19.6±1.1	18.5±1.1	5.0±0.4		2.2±0.4	8.3±0.5	4.2±0.2	1.7±0.4	20.6±1.2	15.4±0.9		4.4±0.4
0.2	8.2±1.2	30.8±3.7	3.4±0.5		4.9±2.4	6.1±0.8	3.9±1.0	6.3±1.3	15.6±1.8	10.3±1.8	4.5±0.7	6.1±0.8
0.25	10.9±2.1	23.4±4.5	3.1±0.8	1.9±1.1	6.4±1.5	2.2±0.7		5.3±2.9	27.2±7.4	11.9±2.6	2.0±0.8	3.7±0.9
0.333	29.8±1.0	6.2±0.7	5.7±0.4		8.2±0.4	2.0±0.2	0.3±0.5		28.9±1.3	11.3±0.7	2.7±0.2	4.4±0.5
4 wt.% H_2O:												
0	3.2±0.3	9.9±0.7	2.1±0.1		6.9±0.5	3.1±0.1		18.1±1.1	6.2±0.4	5.5±0.5	2.2±0.3	5.9±0.5
5 wt.% H_2O:												
0	37.6±2.1	12.5±0.7	1.9±0.4		5.4±0.5	4.8±0.4		22.0±1.6	3.9±0.3	2.3±0.3	2.6±0.3	2.1±0.1
0.125	8.3±2.1	10.7±0.7	2.7±0.4		2.0±0.5	7.8±0.3	4.3±0.4	3.5±0.4	14.0±1.0	13.0±0.9	0.7±0.1	3.9±0.1
0.2	22.4±1.4	18.2±1.2	6.1±0.4		7.1±0.9	4.9±0.4	3.6±0.3	2.5±0.4	19.5±1.2	9.4±0.7	2.5±0.2	5.8±0.5
0.25	14.4±0.6	15.0±0.6	6.2±0.3		9.2±0.6	2.2±0.2		5.8±0.4	29.7±1.0	11.0±0.6	2.9±0.1	3.6±0.2
0.333	13.1±0.8	19.7±1.2	4.7±0.5		9.8±0.6	2.8±0.9	0.9±0.1		28.9±1.7	15.0±0.9	2.7±0.3	2.4±0.1
7.5 wt.% H_2O:												
0	36.4±2.0	11.2±0.7	2.5±0.4		1.9±0.5	10.4±0.8		30.9±1.8	7.4±0.5	3.7±0.4	4.0±0.6	12.5±0.9
10 wt.% H_2O:												
0	31.3±1.7	9.9±0.6	1.7±0.1		6.7±0.5	3.4±0.3		6.3±1.6	5.6±0.4	4.2±0.4	3.2±0.4	8.1±0.6
0.125	31.4±1.8	8.2±0.5	3.4±0.3		3.4±0.4	7.1±0.6	1.5±0.1	7.1±0.7	2.8±0.3	26.9±1.5	0.6±0.1	4.4±0.4
0.2	23.9±1.3	8.3±0.6	5.3±0.4		9.2±0.5	3.3±0.3	4.3±0.3	3.3±0.2	23.2±1.2	10.7±0.6	2.9±0.2	5.6±0.3
0.25	24.2±1.2	8.2±0.5	3.1±0.2		7.1±0.6	3.8±0.3	1.8±0.3	3.5±0.3	30.3±1.5	6.1±0.4	2.6±0.2	9.3±0.5
5 wt.% D_2O:												
0	36.6±2.0	8.8±0.6	1.7±0.3		6.7±0.5	4.8±0.3		10.3±0.7	5.6±0.4	6.2±0.5	3.2±0.3	
0.125	22.5±1.2	15.6±0.9	5.0±0.4		8.5±0.9	6.6±0.5	1.7±0.3	7.2±0.5	12.6±0.7	14.1±0.8	6.3±0.4	
0.2	25.4±1.8	14.5±1.15	0.8±0.5		6.0±0.74±0.4	1.5±0.4	3.2±0.4	24.1±2.6	12.6±1.1	2.5±0.5		
0.25	21.5±1.1	9.0±0.5	3.4±0.3			8.0±0.3	2.2±0.1	1.0±0.1	3.1±0.2	14.0±0.8	36.5±1.8	1.4±0.2

OH bond may exist in SiO_2–H_2O quenched melts (or glasses) remains open to further investigation.

In the spectra of $CaAl_2O_4$–SiO_2–H_2O samples there is no visually well-defined band near 970 cm^{-1} in contrast to SiO_2–H_2O melts (see Fig. 3). However, there is an increase in intensity in this general frequency region. This intensity results in one or two bands fitted near 960-cm^{-1} (also denoted ν_{970} in this text) and 900 cm^{-1} (ν_{900}), depending on the Al/(Al+Si). In contrast to the behavior of the 970-cm^{-1} band in hydrous silica glasses, the ν_{970} band (or bands) does not shift significantly in frequency as H_2O is substituted with D_2O (Figs. 8 and 9; see also Table II).

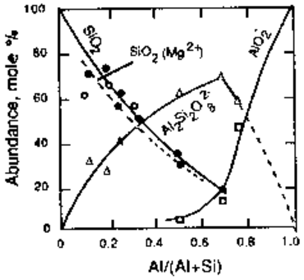

Fig. 5. Abundance of three-dimensional structural units in anhydrous $CaAl_2O_4$–SiO_2 melts as a function of Al/(Al+Si) (data from Seifert et al., 1982).

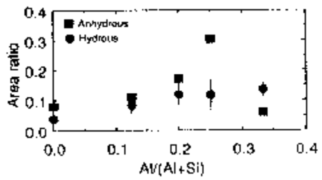

Fig. 6. Area of ν_{600} band relative to the area of $\nu_{600}+\nu_{440}+\nu_{490}$ for hydrous and anhydrous melts as a function of their Al/(Al+Si).

In the spectra of the most water-rich samples, the band can be deconvoluted into two, one near 970 cm^{-1} (ν_{970}) and one near 900 cm^{-1} (ν_{900}) as shown, for example, in Fig. 4B. There are no systematic relationships between the frequency of the ν_{900} band and substitution of deuterium for hydrogen in the water (Fig. 8A). A similar Raman band near 900 cm^{-1} occurs in hydrous melts on the join $NaAlO_2$–SiO_2 (McMillan and Remmele, 1986; Mysen and Virgo, 1986a) and has also been reported in infrared spectra of quenched melts on this join (Silver and Stolper, 1989).

In the $NaAlO_2$–SiO_2–H_2O melts, the 900-cm^{-1} band was assigned to nonbridging oxygen (Mysen and Virgo, 1986a). However, McMillan and Remmele (1986), as adopted by Silver and Stolper (1989), suggested that the 900-cm^{-1} band could be assigned to (Si,Al)–OH stretching. In the latter reports, its lower frequency compared with the 970-cm^{-1} Si–OH stretch band in SiO_2–H_2O (Stolen and Walrafen, 1976) was rationalized as resulting from the Al⇌Si substitution. However, this suggested assignment is not likely because both in the Raman spectra of melts on the join $NaAlO_2$–SiO_2–H_2O (Mysen and Virgo, 1986a) and those observed for $CaAl_2O_4$–SiO_2–H_2O here (Table II), the frequency of the ν_{900} band does not vary as predicted when ^2H substituted for ^1H in the water. An ~10-cm^{-1} frequency reduction of the ν_{900} band would be expected from the relationship (Freund, 1982):

$$\nu^{SiOH}/\nu^{SiOD}=(m^{SiOD}/m^{SiOH})^{1/2} \quad (1)$$

where ν = frequency, with $\nu^{SiOD}/\nu^{SiOH}=1.011$; and m = oscillator mass. For an equivalent Al-OH bond, the ratio is 1.0113. If the ν_{900} band is due to (Si,Al)–OH stretching at 900 cm^{-1}, the same band should be at 890 cm^{-1} with the same concentration of D_2O in substitution for H_2O. However, there is no evidence of such a frequency shift. This analysis, which is identical to that by Mysen and Virgo (1986a), leads to the conclusion that the 900-cm^{-1} band is not due to (Si,Al)–OH. Therefore, the alternative interpretation that the band is due to nonbridging oxygen is the assignment in the present melt compositions.

The frequencies of the 900-cm^{-1} band generally decrease with increasing water content (Fig. 8) at constant Al/(Al+Si) with the exception of the *CA2S4* composition melt [Al/(Al+Si)=0.333] where the opposite trend is observed (Table II). This behavior differs from the 900-cm^{-1} band in $NaAlO_2$–SiO_2 where there is a systematic increase in its frequency with increasing water content. The ν_{900} band, which was not observed in the hydrous $NaAlO_2$–SiO_2 melts, exhibits similar functional relationships to H_2O concentration and Al/(Al+Si) (Fig. 9). The frequency decrement of these bands with either H_2O or Al/(Al+Si) can be explained as the result of increased Al/(Al+Si) in the structural units that give rise to the ν_{970} and ν_{900} bends.

The intensity relations among the 970-, 1150- and 1200-cm^{-1} bands together with their

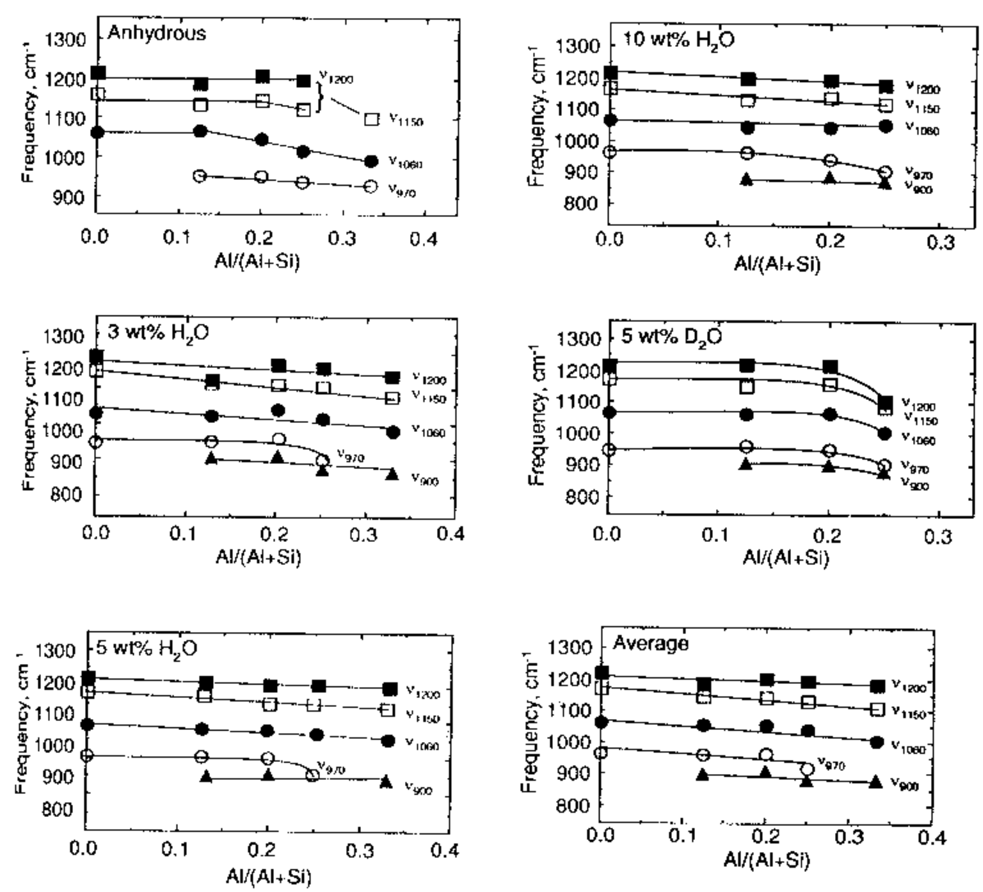

Fig. 7. Raman frequencies of important bands in the high-frequency segments of the low-frequency portion of spectra as a function of Al/(Al+Si) at total water concentrations indicated. The average values are for all the H_2O contents (the samples with D_2O are not included).

frequency relationships as a function of Al/(Al+Si) and H_2O concentration are of interest because there are at least three different possible assignments of the 970-cm^{-1} band:

(1) There is a band near 970 cm^{-1} in anhydrous calcium aluminate-silica melts (McMillan et al., 1982; Seifert et al., 1982) that is part of the signature of the three-dimensionally interconnected network. The ν_{970} band intensity in anhydrous $CaAl_2O_4$–SiO_2 melts is insensitive to Al/(Al+Si) (Fig. 10A), whereas in hydrous melts, the area ratio, $A_{970}/(A_{970}+A_{1150}+A_{1200})$, tends to increase with Al/(Al+Si) (Fig. 10B) in particular with the lowest water contents (3 wt.%). From this different behavior of the ν_{970} band in anhydrous vs. hydrous $CaAl_2O_4$–SiO_2 melts it would appear that the ν_{970} band in hydrous calcium al-

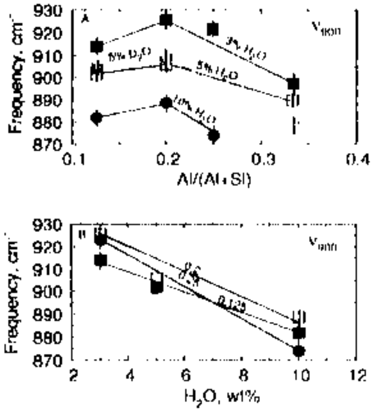

Fig. 8. Frequencies of ν_{900} band as a function of Al/(Al+Si) at constant H_2O content (A) and as a function of total water content at Al/(Al+Si) (B) indicated on lines. *Shaded squares* are from D_2O samples.

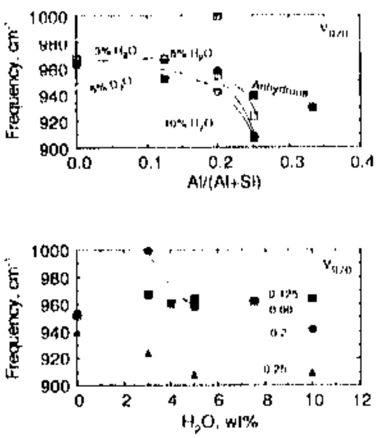

Fig. 9. Frequencies of ν_{970} band as a function of Al/(Al+Si) at constant H_2O content (A) and as a function of total water content at Al/(Al+Si) indicated on lines. *Shaded squares* are from D_2O samples. The lines from 0 to 3 wt.% H_2O are *dashed* as it is not likely that the ν_{970} band in spectra of anhydrous samples is the same band as in the hydrous equivalents.

uminosilicate melts is not the same band as that near 970 cm^{-1} in the anhydrous equivalents.

(2) As observed in the spectra of quenched

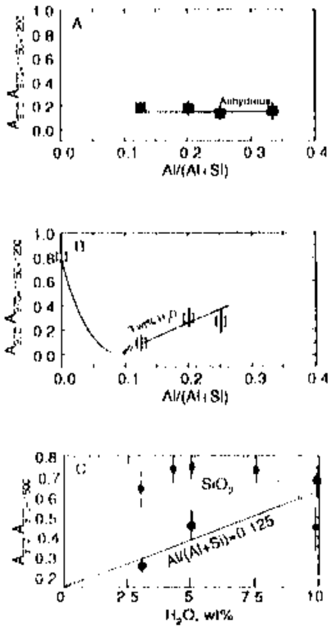

Fig. 10. Selected area ratios involving the ν_{970} bands as a function of H_2O contents for compositions indicated. The data point for Al/(Al+Si) in (B) is connected with *dashed arrow* as it is not likely that this band is the same as in the Al-bearing samples. The $A_{970}/(A_{970}+A_{1600})$ for Al-bearing SiO_2–H_2O quenched melt in (C) is shown as *shaded* for comparison.

melts in the system SiO_2–H_2O (Fig. 3), Si–OH stretch vibrations also are near 970 cm^{-1} (e.g., Stolen and Walrafen, 1976). The behavior of the 970-cm^{-1} band in Al-free SiO_2–H_2O melts (where it is assigned to Si–OH stretching) differs from its behavior in Al-bearing materials in two important ways. Both the $A_{970}/(A_{970}+A_{1150}+A_{1200})$ and the $A_{970}/(A_{970}+A_{1600})$ area ratios are significantly higher in the Al-free (SiO_2–H_2O) melts (Table V). Furthermore, whereas in SiO_2–H_2O melts the $A_{970}/(A_{970}+A_{1600})$ is insensitive to H_2O concentration and may actually decrease with the highest water content, this area ratio increase with water content in the aluminous samples (Fig. 10C). Finally, in SiO_2–H_2O

melts the frequency of the 970-cm^{-1} band is sensitive to ^{2}H substitution for ^{1}H, whereas in Al-bearing melts, no frequency dependence of the atomic wright of hydrogen was observed. Therefore, the behavior of the ν_{970} band in the hydrous $CaAl_2O_4$–SiO_2 melts is difficult to reconcile with an assignment to (Si,Al)–OH stretching.

(3) Finally, it is possible that this band reflects (Si,Al)–O$^-$ (O$^-$ denotes nonbridging oxygen) formed in these originally fully polymerized melts through interaction with H_2O.

In light of the differences with anhydrous $CaAl_2O_4$–SiO_2 melts on the one side and with SiO_2–H_2O on the other, it appears reasonable that the ν_{970} band in $CaAl_2O_4$–SiO_2–H_2O melts at least to a degree has a contribution from nonbridging oxygen. The intensity variations as a function of Al/(Al+Si) and H_2O content lead to the suggestion that: (1) if there is Si–OH or (Si, Al)–OH bonding the contribution from (Si,Al)–O$^-$ relative to either Si–OH or (Si,Al)–O^0, or both, varies with Al/(Al+Si) and H_2O concentration; or (2) alternatively, in hydrous calcium aluminosilicate melts the band is controlled by structural features that are absent in SiO_2–H_2O and in anhydrous $CaAl_2O_4$–SiO_2 melts. For example, the decreasing frequency with increasing Al/(Al+Si) in the hydrous melts could be explained by increasing Al/(Al+Si) in the depolymerized structured unit that contributes (in part or in full) to the behaviour of this band. Whether alternative (1) or (2) represents the correct interpretation cannot be ascertained from the high-frequency segments of the the 300–1800-cm^{-1} spectral region alone.

3.2. High-frequency region

The high-frequency envelope (3000–4000 cm^{-1}) is broad and asymmetric with a tail toward lower frequencies (Figs. 3C and 4C). The bands in this envelope are the fundamental O–H stretch vibrations, the frequencies of which are sensitive to the electronic properties of the metal cation to which the OH group is at tached and to hydrogen bonding.

The equivalent envelope for deuterated samples occurs between 2000 and 3000 cm^{-1}. The frequency differences between the OH and OD stretching bands result from the relationship between oscillator mass and frequency for a two-atom group (Langer and Lattard, 1980):

$$\nu = (f/2\pi c)^{1/2}(1/m_1 + 1/m_2) \quad (2)$$

where ν is the frequency; f is the force constant; c is the speed of light; and m_1 and m_2 are the atomic masses of the oscillators. It has been found (Hartwig, 1977; Langer and Lattard 1980), that the frequency ratio, $\nu_{OH}/\nu_{OD} = 1.37$. From this relationship, a maximum Raman intensity near 3600 cm^{-1} for OH corresponds to 2600 cm^{-1} for OD.

The spectra from the SiO_2–H_2O melts are better resolved than those from the Al-bearing samples and typically two peaks can be discerned visually near 3600 cm^{-1} (Fig. 3C). In aluminous samples, visual inspection reveals only one sharp band with a shoulder on its high-frequency side.

The best fit is generally obtained with four bands fitted to all the spectra. The two highest frequency bands (ν_{3600} and ν_{3650}) are quite sharp with full widths at half height (FWHH) for the Al-free samples of 33 ± 6 and 34 ± 3 cm^{-1}, respectively (averaged over all the water-bearing silica glasses). These two bands are somewhat broader in Al-bearing samples (FWHH is 82 ± 21 and 48 ± 14 cm^{-1} for the ν_{3600} and ν_{3650} bands, respectively, averaged over all H_2O and Al contents). The FWHH-values of the two highest frequency bands in the deuterated samples are comparable to those of the H_2O-bearing materials (80 ± 13 and 39 ± 2 cm^{-1}, respectively). The FWHH-values of the two lowest-frequency bands (ν_{3300} and ν_{3500}) are considerably greater (197 ± 66 and 116 ± 26 cm^{-1} for SiO_2 and 128 ± 33 and 109 ± 36 for Al-bearing samples, respectively) than those of the ν_{3600} and ν_{3650} bands. In the system SiO_2–H_2O, the frequencies of the ν_{3300}

and ν_{3500} bands decrease with water content (Fig. 11A). In contrast, there is no clear functional relationship between the ν_{3300} and ν_{3500} frequencies and water content in the spectra of hydrous, aluminous samples (Fig. 11B). However, all the band frequencies are negatively correlated with Al/(Al+Si) (Fig. 11C) with a slight, but distinctive decrease in ν_{3600} and ν_{3650} frequency as the samples become more aluminous. The ν_{3300} and ν_{3500} frequencies are somewhat more sensitive to Al/(Al+Si) than those of ν_{3600} and ν_{3650} (Fig. 11C), as also found for hydrous melts in the system $NaAlO_2$–SiO_2 (Mysen and Virgo, 1986a).

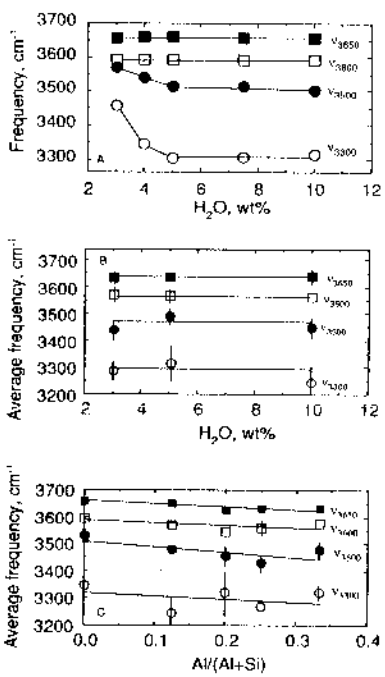

Fig. 11. Frequencies of fundamental OH stretch bands in SiO_2–H_2O as a function of water content (A), average values for all Al-bearing samples as a function of H_2O content (B), and average values of all Al-bearing samples as a function of Al/(Al+Si) (C). *Error bars* represent standard error of the average values. Error bars are not shown when error is less than the symbol size.

Visual inspection of the the spectra reveals a rapid growth over a broad frequency region <3600 cm^{-1} as the water content increases (Figs. 3C and 4C). For all compositions, this observation results from the general intensity increase of the two lowest-frequency bands (ν_{3300} and σ_{3500}) and a complementary decrease in intensity of the two highest-frequency bands (ν_{3600} and ν_{3650}) with increasing water content (Figs. 12 and 13).

From eq. 2, the frequencies of the four bands in the high-frequency portion of the D_2O spectra relate to the four bands from the H_2O-bearing samples with frequency ratios quite similar to the theoretically predicted value [the average ν^{OH}/ν^{OD} in the Al/(Al+Si) range for which data have been obtained (0–0.25) for the bands are 1.39, 1.36, 1.36 and 1.35, for ν_{2300}/ν_{3300}, ν_{2500}/ν_{3500}, ν_{2600}/ν_{3600} and ν_{2650}/ν_{3650}, respectively]. Thus, the four bands in the 2000–3000-cm^{-1} envelope for D_2O samples (ν_{2300}, ν_{2500}, ν_{2600} and ν_{2650}) have the same spectral characteristics and may be equivalent to the four bands in the 3000–4000-cm^{-1} envelope in H_2O samples (ν_{3300}, ν_{3500}, ν_{3600} and ν_{3650}).

The four bands in the spectra of hydrous silica melts can be assigned to OH stretching in OH groups from Si–OH bonds (ν_{3650} and ν_{3600}) and from OH groups in molecular H_2O (ν_{3300} and ν_{3500}). In the SiO_2–H_2O system, this assignment is consistent with the observations that: (1) the frequencies of the ν_{3650} and ν_{3600} bands are independent of H_2O concentration: and (2) the relative intensity of the ν_{3300} and ν_{3500} bands increases significantly with increasing H_2O concentration (Figs. 11A and 12). The frequency decrease with H_2O content of the two lowest-frequency bands in SiO_2–H_2O is consistent with greater importance of hydrogen bonding among water molecules as the total water content is increased. Hydrogen bonding will lower the O..H bond strength. Systematic frequency reduction of OH stretch bands as a function of the strength of hydrogen

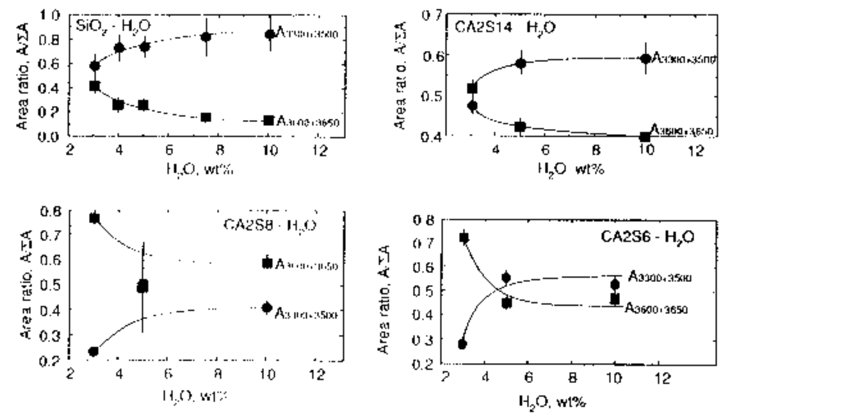

Fig. 12. Relative area of the two low-frequency (ν_{3300} and ν_{3500}) and the two high-frequency (ν_{3600} and ν_{3650}) bands relative to the complete scattering intensity of the OH stretch band envelope as a function of H_2O content for compositions indicated. $\Sigma A = A_{3300} + A_{3500} + A_{3600} + A_{3650}$.

bonding is well documented (Nakamoto et al., 1955), as also recently demonstrated for hydroxyl-bearing minerals (Dobson et al., 1989). Increased hydrogen bonding lowers the OH bond strength lowering the OH stretch force constant and, therefore, the frequency. The comparatively rapid frequency reduction of the ν_{3300} and ν_{3500} bands in the spectra of quenched SiO_2–H_2O melts with water concentration (Fig. 11A) may be due to the influence of hydrogen bonding.

Although the overall frequency and intensity trends in aluminous samples resemble those in SiO_2–H_2O, there are some important differences. In the spectra of the Al-bearing materials: (1) the frequencies of the ν_{3650} and ν_{3600} bands show a small, but systematic decrease with increasing Al/(Al+Si) of the melt (Fig. 11C); (2) the ν_{3650} and ν_{3600} bands are significantly broader than in SiO_2–H_2O; and (3) in contrast to the SiO_2–H_2O system (Fig. 11A), *all* the band frequencies are independent of total H_2O content regardless of Al/(Al+Si) of the melt (Fig. 11B).

The negative correlation (Fig. 11) between ν_{3300}, ν_{3500}, ν_{3600} and ν_{3650} band frequencies and Al/(Al+Si) may be rationalized by considering the electronic properties of the metal cation (M) in possible M–OH bonds in the melts. The frequency reduction of the ν_{3650} and ν_{3600} bands with increasing Al/(Al+Si) might reflect a weakening of the O–H bonds resulting from substitution of Al^{3+} for Si^{4+} to form (Si,Al)–OH or Al–Oh bonds in the samples. However, this interpretation somewhat difficult to reconcile with the behavior of the ν_{970} band in $CaAl_2O_4$–H_2O melts (see also discussion on pp. 233–235) unless this latter band also has a contribution from (Si,Al)–OH stretching. For example, the 970-cm^{-1} band did not, however, show the expected frequency-dependence of deuterium substitution for hydrogen (Fig. 9). A ~13-cm^{-1} frequency reduction is expected from eq. 1 (as observed in SiO_2–H_2O vs. SiO_2–D_2O $\Delta\nu^{D/H} = 15 \pm 3$ cm^{-1}; see Table II) if the ν_{970} band was assigned to (Si,Al)–OH stretching in the aluminous samples. The observed frequency of the ν_{970} band is reduced by $\lesssim 5$ cm^{-1} (Fig. 9), which is barely outside the uncertainty in the fitted line positions (typically $\pm$1–4 cm^{-1}). One cannot rule out some (Si,Al)–OH in these

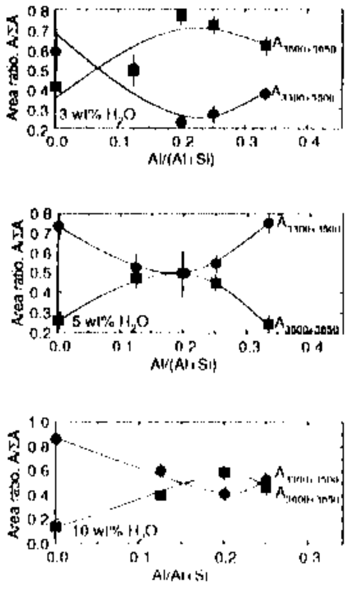

Fig. 13. Relative area of the two low-frequency (ν_{3300} and ν_{3500}) and the two high-frequency (ν_{3600} and ν_{3650}) bands relative to the complete scattering intensity of the OH stretch band envelope as a function of Al/(Al+Si) for the H_2O concentrations indicated. $\sigma A = A_{3300}+A_{3500}+A_{3600}+A_{3650}$.

melts, but the contribution from such bonds must be comparatively small. With regards to the spectral topology in the 3000–4000 cm^{-1} region, it is suggested that a small fraction of the structurally bound OH could be a mixed (Si,Al)–O(OH) tetrahedral environment, or there may be mixtures of Si–OH and Al–OH, where the frequencies of the respective OH stretch bands in the 3600-cm^{-1} envelope could not be resolved with the fitting procedure. The considerably greater line width of the ν_{3650} and ν_{3600} bands in spectra of the aluminous could be interpreted as consistent with the latter suggestion.

The two bands lower-frequency bands (ν_{3300} and ν_{3500}) could be due to OH stretching in molecular water. Their increased intensity with increasing water content is consistent with an increased abundance of molecular H_2O in these samples (as inferred from infrared (IR) and NMR spectroscopy; e.g., Stolper, 1982; Eckert et al., 1988). The presence of molecular H_2O is also consistent with the distinctive H–O–H bending mode, with a frequency near 1600 cm^{-1}, in all hydrous samples from the join $CaAl_2O_4$–SiO_2 (Fig. 4B; see also Tables II and III). The observation that the frequency of the 1600-cm^{-1} band is insensitive to water content (Table II) suggests that water polymerization in the melt does not vary with amount of water present (Paterson, 1982). This suggestion is consistent with [1]H NMR information (Eckert et al., 1988) which indicates that the H_2O molecules in aluminosilicate glasses are isolated.

However, the behavior of the ν_{3300} and ν_{3500} bands in hydrous silica and hydrous CaA_2O_4–SiO_2 melts differs in that in SiO_2–H_2O quenched melts where their frequencies decrease with increasing water concentration, whereas those from $CaAl_2O_4$–SiO_2–H_2O do not (Fig. 11A and B). In the latter compositions, the ν_{3300} and ν_{3500} band frequencies decrease slightly with Al/(Al+Si) (Fig. 11C). The frequency shift could be interpreted to result from increased hydrogen bond strength as the melts become more aluminous. If so, in analogy with SiO_2–H_2O (Fig. 11A) one would also expect a water concentration dependence of the band frequencies, which is not observed for these compositions. An alternative is that in addition to some intensity contribution from OH groups in H_2O, this frequency region also has contributions from OH groups bonded to other metal cations (Ca^{2+}, or Al^{3+}, or both). This interpretation is consistent with observations (Mysen and Virgo, 1986b) that in melts on the job Na(OH)–SiO_2 with NaOH concentration equivalent to 1.35 wt.% H_2O [a water concentration range whether neither IR nor Raman spectroscopy indicate a significant amount of molecular H_2O present (Mysen and Virgo, 1986b; Silver and Stolper, 1989), the intensity of the ν_{3300} and ν_{3500} band is > 50% of the entire OH stretch envelope. In the system SiO_2–Al(OH)$_3$ with Al(OH)$_3$ concentration equivalent to 2.5 wt.% H_2O where, regardless of which model of water speciation is chosen, no more than 0.5% of the species is molecular H_2O, the ν_{3500} band also represents near 50% of the intensity in the OH stretch envelope. Thus, there is evidence that at least a portion of the two low-frequency intensities may have contributions from OH stretching from both Al–OH and Ca–OH bonds in addition to H–OH. It is likely that all three forms of OH (H...OH, Al...OH and Ca...OH) exist in the melts and contribute to this portion of the spectrum, but that the individual bands could not be resolved with the fitting procedure.

4. Discussion

The interpretation of the Raman spectra of quenched melts on the join $CaAl_2O_4$–SiO_2–H_2O is consistent with water dissolved as molecular H_2O and in the form of various OH complexes. Before discussing possible detailed solubility mechanisms, it should be noted that in the present paper as well as elsewhere in the literature, the spectra were obtained from temperature-quenched melts (hydrous glass) with quenching rates of the present experiments shown in Fig. 2. However, the proportion of various OH complexes (including molecular H_2O) may depend on the conditions of temperature quenching where the quenching rates, for example, could affect the interpretation of the results (Dingwell and Webb, 1989a, b).

Stolper and coworkers in several reports (e.g., Stolper, 1982; Silver and Stolper, 1989) suggested that the water speciation is only weakly temperature dependent. On the other hand, Dingwell and Webb (1989a, b) suggested that speciation in silicate melts in general, and OH^-/H_2O in particular, was significantly temperature-dependent. Dingwell and Webb (1989b) calculated from relaxation theory, for example, that for a reaction:

$$2OH^- \rightleftharpoons H_2O + O^{2-} \quad (3)$$

that could describe the equilibrium between between oxygen in the melt and the two principal forms of water, $\Delta H = 25 \pm 5$ kJ mol^{-1}. They concluded that OH^-/H_2O measured from quenched materials is that frozen in near the glass transition temperature, and that at the temperature of *equilibration*, nearly all the dissolved water exists in the OH^- form. In contrast, Silver and Stolper (1989) suggested that reaction (3) was only weakly temperature-dependent. Unfortunately, until in situ, high-temperature, high-pressure spectroscopy of hydrous melts is carried out, this controversy will remain unresolved, and measurements of OH^-/H_2O of quenched melts should be viewed with these possible problems in mind.

The spectra of $CaAl_2O_4$–SiO_2–H_2O composition quenched melts are consistent with the existence of several different M...OH complexes. The absence of a clear 970-cm^{-1} band that could be assigned to Si–OH [or (Si,Al)–OH] stretching leads to the suggestion that OH groups bonded to Si^{4+} are not of major importance in aluminosilicate melts — a conclusion also reached by McMillan and Remmele (1986) and Mysen and Virgo (1986a) for melts in the system $NaAlO_2$–SiO_2–H_2O. However, the band near 970 cm^{-1} (and that near 900 cm^{-1} for certain compositions) in the $CaAl_2O_4$–SiO_2–H_2O quenched melts could be assigned to (Si,Al)–O$^-$ stretching. That is, nonbridging oxygens have been formed by solution of H_2O in $CaAl_2O_4$–SiO_2 melts. Nonbridging oxygen could from via two mechanisms. Either OH groups are associated with Ca^{2+} or with Al^{3+}. Due to the ionic character of Ca–OH and Al–OH bonds, the relevant Ca–OH and Al–OH stretch vibrations are likely to occur at frequencies ≲600 cm^{-1} (e.g., Nakamoto, 1978), where the spectral resolution is poor, and this portion of the Raman spectra cannot be used with confidence for such assignments. Therefore, the existence of such OH complexes in the melts was inferred from the topology of the 3000–4000-cm^{-1} envelope in this discussion above.

Neither the discussion of the 970-cm^{-1} band nor that of the bands in the 3000–4000-cm^{-1} envelope yields direct information about the relative importance of Ca^{2+} and Al^{3+} complexing with OH in the melts. In principle, the proportion of the various complexes governs the extent to which a fixed amount of dissolved water depolymerizes the melt. One can write, for example, idealized end-member reactions that relate the formation of each of these OH complexes separately to the formation of nonbridging oxygen in the melt (NBO). For the formation of $Ca(OH)_2$ (Ca..OH complexing), the reaction is:

$$Ca_nAl_{2n}Si_{2m}O_{4(n+m)}+nH_2O\rightleftharpoons$$
$$nCa(OH)_2+2nAl^{3+}+3nSiO_3^{2-}$$
$$+(2m-3n)SiO_2 \qquad (4)$$

and for $Al(OH)_3$ (Al..OH complexing) formation, it is:

$$Ca_nAl_{2n}Si_{2m}O_{4(n+m)}+3nH_2O\rightleftharpoons$$
$$2nAl(OH)_3+nCa^{2+}+nSiO_3^{2-}$$
$$+(2m-n)SiO_2 \qquad (5)$$

If water dissolved by replacing a bridging oxygen in the aluminosilicate network [(Si,Al)O(OH)], one can write a reaction analogous to that proposed by Burnham (1974, 1975) for $NaAlSi_3O_8$ melt:

$$Ca_nAl_{2n}Si_{2m}O_{4(n+m)}+\tfrac{3}{2}nH_2O\rightleftharpoons$$
$$nCa(OH)_2+Al_{2n}Si_{2m}O_{4m+3n}(OH)_n \qquad (6)$$

For reaction (4), 6 nonbridging oxygens will be formed per molecule H_2O dissolved in the melt as $Ca(OH)_2$, whereas for reaction (5) $\tfrac{2}{3}$NBO will be formed per molecule H_2O dissolved as $Al(OH)_3$. No nonbridging oxygens are formed in reaction (6). This effect of dissolved water on the melt structure, also found for melts in the system $NaAlO_2$–SiO_2–H_2O (Mysen and Virgo, 1986a), is the result of the need to charge-balance tetrahedrally-coordinated Al^{3+} with Ca^{2+}. Thus, if one Ca^{2+} interacts with H_2O to form $Ca(OH)_2$, two Al^{3+} originally in tetrahedral coordination in anhydrous melt become network modifiers. Each of these Al^{3+} cations expelled from the tetrahedral network can stabilize three nonbridging oxygens. Thus, for each $Ca(OH)_2$ formed by this mechanism, 6 nonbridging oxygens are formed. If, on the other hand, $Al(OH)_3$ complexes are formed, one Ca^{2+} will become network-modifying for two Al^{3+} forming $Al(OH)_3$. Thus, 2 nonbridging oxygens will be stabilized the melt per two $Al(OH)_3$ complexes formed by interaction between Al^{3+} and H_2O. This reaction requires three H_2O, and, thus $\tfrac{2}{3}$NBO will be formed per molecule H_2O dissolved as $Al(OH)_3$.

The number of nonbridging oxygens per molecule dissolved H_2O as an OH complex not bonded to H in reactions (3) and (4) is independent of the Al/(Al+Si). However, the degree of polymerization expressed as nonbridging oxygens per tetrahedrally coordinated cations (NBO/T), does depend on the Al/(Al+Si) because the abundance ratio, SiO_2/SiO_3^{2-}, is a function of n/m (Table VI) so that the more aluminous the melt by more rapidly will the NBO/T increase with water dissolved as either $Ca(OH)_2$ or $Al(OH)_3$. Moreover, by dissolving water in the form of $Ca(OH)_2$ rather than $Al(OH)_3$, the rate of melt depolymerization with increasing water content is greater.

In order to evaluate the relative importance

TABLE VI

Rate of change of NBO/T with H_2O concentration in OH complexes [$\partial(NBO/T)/\partial H_2O$]

Al/(Al+Si)	$\partial(NBO/T)/\partial(H_2O)$ (mol^{-1})		
	(Si,Al)O(OH)	$Al(OH)_3$	$Ca(OH)_2$
0.125	0	$\frac{1}{9}$	$\frac{1}{2}$
0.200	0	$\frac{1}{6}$	$\frac{3}{4}$
0.250	0	$\frac{2}{9}$	1
0.333	0	$\frac{1}{3}$	3

of the three idealized reaction above [reactions (4–6)] it is necessary to determine the NBO/T and the abundance ratio, OH/H_2O, in the melts. In principle, the value of NBO/T can be determined from area ratios such as $A_{900}/(A_{900}+A_{1150}+A_{1200})$ and $A_{970}/(A_{1150}+A_{1200})$ where the A_{900} and A_{970} are the areas of the Raman bands from nonbridging oxygens. These area ratios have been calibrated against NBO/T in the systems Na_2O–SiO_2 and K_2O–SiO_2 (Mysen, 1990). Such a calibration factor, θ, for a given area [e.g., $A_{900}{}^R=A_{900}/(A_{900}+A_{1150}+A_{1200})$], could then be used to determine the abundance of nonbridging oxygens in that unit, $X_{900}{}^{NBO/T}$:

$$X_{900}{}^{NBO/T}=\theta A_{900}{}^R \qquad (7)$$

However, it is not well established how these calibration factors may be affected by Al^{3+} substituted for Si^{4+} in the structural units of interest. It is known (Sharma and Simons, 1981) that the intensity of the ν_{1150} and ν_{1200} bands increase with increasing Al/(Al+Si). Thus, in the spectra reported here, the relevant intensity ratios for a given bulk melt NBO/T are likely to be smaller than in equivalent Al-free melts, and the calibration factor from the Al-free systems would underestimate the mole/fractions (i.e. inferred values of $X_{900}{}^{NBO/T}$ from eq. 7). If it is assumed, nevertheless, that the θ for SiO_3^{2-} units from Mysen (1990) is applicable to both the ν_{900} and ν_{970} bands ($\theta=1.4$), the NBO/T-values for the melts studied here would be in the range between ~0.25 and ~0.5. By assuming that θ is independent of composition, the NBO/T from the area data in Table V is independent of H_2O in the water concentration range studied. This conclusion is only reasonable if: (1) either the H_2O in melts with >3 wt.% H_2O is dissolved either according to reaction (6), or (2) the additional water is dissolved in molecular form. Furthermore, because, with the exception of the 10-wt.% H_2O isochore, the $A_{900}/(A_{900}+A_{1150}+A_{1200})$ decreases with Al/(Al+Si) and the $A_{970}/(A_{970}+A_{1150}+A_{1200})$ only increases slowly with Al/(Al+Si) (see Table V), the NBO/T of a melt for a given water content would decrease as the melts become more aluminous. The latter trend was also observed in the system $NaAlO_2$–SiO_2–H_2O (Mysen and Virgo, 1986a), and was ascribed to a positive correlation between Al/(Al+Si) and $Al(OH)_3$/NaOH in the OH complexes in the melts. It would appear from the present data that in the system $CaAl_2O_4$–SiO_2–H_2O an analogous relation [positive correlation between $Al(OH_3/Ca(OH)_2$ in the OH complexes and bulk melt Al/(Al+Si)] exists. Thus, the more aluminous aluminosilicate melts with Ca-charge-balanced tetrahedrally-coordinated Al^{3+}, the less efficiently will dissolved H_2O depolymerize the melt. This trend is more pronounced the lower the total water content of the melt.

In summary, water is dissolved in calcium aluminoslicate melts to form OH complexes with *all* the cations present (including H^+), but probably with Ca complexing dominating in the Ca-aluminosilicate melts similar to the predominantly Na..OH complexing in Na-aluminosilicate melts. In contrast to the spectroscopic observations from melts in the $NaAlO_2$–SiO_2 system (Mysen and Virgo, 1986a), (Si,Al)–OH bonding cannot be ruled out. However, if such bonds are present, their abundance relative to other OH bonding in the melts is relatively unimportant. In both Na- and Ca-aluminosilicate melts, the Al–OH bonds become more important relative to Ca–OH (or Na–OH) as the melts become more aluminous. This trend results in less efficient depolymerization of the melts the more aluminous they are.

Acknowledgements

Critical reviews by C.T. Prewitt, H.S. Yoder, Jr. and two anonymous reviewers are appreciated.

References

Boyd, F.R. and England, J.L., 1960. Apparatus for phase equilibrium measurements at pressures up to 50 kilobars and temperatures up to 1750°C. J. Geophys. Res., 65: 741–748.

Burnham, C.W., 1975. Thermodynamics of melting in experimental silicate–volatile systems. Geochim. Cosmochim. Acta, 39: 1077–1084.

Burnham, C.W., 1974. $NaAlSi_3O_8$–H_2O solutions: A thermodynamic model for hydrous magmas. Bull. Soc. Fr. Minéral. Cristallogr., 97: 223–230.

Carmichael, I.S.E., Turner, F.J. and Verhoogen, J., 1976. Igneous Petrology. McGraw-Hill, New York, N.Y., 739 pp.

Chayes, F., 1975a. Average composition of the commoner Cenozoic volcanic rocks. Carnegie Inst. Washington Yearbk., 74: 547–549.

Chayes, F., 1975b. A world data base for igneous petrology. Carnegie Inst. Washington Yearbk., 74: 549–550.

Davidson, W.C., 1966. Variable Metric Method for Minimization. Argonne Natl. Lab. ANL 5990 3rd rev. ed. Lawrence Livermore Natl. Lab., Livermore, Calif.

Dingwell, D.B. and Mysen, B.O., 1985. Effects of water and fluorine on the viscosity of albite melt at high pressure: a preliminary investigation. Earth Planet. Sci. Lett., 74: 266–274.

Dingwell, D.B. and Webb, S.L., 1989a. Structural relaxation in silicate melts and non-Newtonian melt rheology in geologic processes. Phys. Chem. Miner., 16: 508–516.

Dingwell, D.B. and Webb, S.L., 1989b. The temperature-dependence of water speciation in rhyolite melts: Analysis of quench-rate dependent speciation using relaxation theory. Eos (Trans. Am. Geophys. Union), 70: 501–502 (abstract).

Dobson, P.F., Epstein, S. and Stolper, E.M., 1989. Hydrogen fractionation between coexisting vapor and silicate glasses and melts at low pressure. Geochim. Cosmochim. Acta, 53: 2723–2731.

Eckert, H., Yesinowski, J.P., Silver, L.A. and Stolper, E.M., 1988. Water in silicate glasses: Quantification and structural studies by ^1H solid echo and MAS NMR methods. J. Phys. Chem., 92: 2055–2064.

Eggler, D.H. and Burnham, C.W., 1984. Solution of H_2O in diopside melts: a thermodynamic model. Contrib. Mineral. Petrol., 85: 58–67.

Epel'baum, M.B., 1985. The structure and properties of hydrous granitic melts. Geol. Carpathica, 36: 491–498.

Epel'baum, M.B., Salova, T.P. and Varshal, B.G., 1975. Influence of water on the coordination of Al^{3+} in water-containing aluminosilicate glasses. Izv. Akad. Nauk S.S.S.R., 8: 1496–1500.

Farnan, I., Kohn, S.C. and Dupree, R., 1987. A study of the structural role of water in hydrous silica using cross-polarisation magic angle NMR. Geochim. Cosmochim. Acta, 51: 2869–2874.

Fletcher, R. and Powell, M.J.D., 1963. A rapidly converging descent method for minimization. Comput. J., [illegible] 163–168.

Freund, F., 1982. Solubility mechanisms of H_2O in silicate melts at high pressures and temperatures: A Raman spectroscopic study: Discussion. Am. Mineral., [illegible] 153–155.

Galeener, F.L., 1982. Planar rings in glasses. Solid State Comm., 44: 1037–1040.

Gaskell, P.H. and Mistry, A.B., 1979. High-resolution transmission electron microscopy of small amorphous silica particles. Philos. J., 39: 245–257.

Hamilton, D.L. and Oxtoby, S., 1986. Solubility of water in albite melt determinated by the weight loss method. J. Geol., 94: 616–630.

Hartwig, C.M., 1977. The radiation-induced formation of hydrogen and deuterium compounds in silica as observed by Raman scattering. J. Chem. Phys., 66: 22[illegible]–239.

Hemley, R.J., Mao, H.K., Bell, P.M. and Mysen, B.O., 1986. Raman spectroscopy of SiO_2 glass at high pressure. Phys. Rev. Lett., 57: 747–750.

Hodges, F.N., 1974. The solubility of H_2O in silicate melts. Carnegie Inst. Washington Yearbk., 73: 251–255.

Kushiro, I., 1978. Density and viscosity of hydrous calc-alkalic andesite magma at high pressure. Carnegie Inst. Washington Yearbk., 77: 675–678.

Kushiro, I., 1989. Evolution of the crust and mantle wedge in Japanese island arcs. Eos (Trans. Am. Geophys. Union), 70: 484 (abstract).

Kushiro, I., Yoder, H.S. and Nishikawa, M., 1968. Effect of water on the melting of enstatite. Geol. Soc. Am. Bull., 79: 1685–1692.

Kushiro, I., Shimizu, N., Nakamura, Y. and Akimoto, S., 1972. Compositions of coexisting liquid and solid phases formed upon melting of natural garnet and spinel lherzolite at high pressures: A preliminary report. Earth Planet. Sci. Lett., 14: 19–25.

Langer, K. and Lattard, D., 1980. Identification of low-energy OH-valence vibration in zoisite. Am. Mineral., 65: 779–883.

Long, D.A., 1977. Raman Spectroscopy. McGraw-Hill, New York, N.Y., 276 pp.

McKeown, D.A., Galeener, F.L. and Brown, G.E., 1984. Raman studies of Al-coordination in silica-rich sodium aluminosilicate glasses and some related minerals. J. Non-Cryst. Solids, 68: 361–378.

McMillan, P.F. and Remmele, R.L., 1986. Hydroxyl sites in SiO_2 glass: A note on infrared and Raman spectra. Am. Mineral., 71: 772–778.

McMillan, P.F., Piriou, B. and Navrotsky, A., 1982. Raman spectroscopic study of glasses along the joins silica – calcium aluminate, silica–sodium aluminate, and silica–potassium aluminate. Geochim. Cosmochim. Acta, 46: 2021–2037.

McMillan, P.F., Peraudeau, G., Holloway, J.R. and Coutures, J.-P., 1986. Water solubility in calcium aluminosilicate melt. Contrib. Mineral. Petrol., 94: 178–182.

Murdoch, J.B., Stebbins, J.F. and Carmichael, I.S.E., 1985. High-resolution ^{29}Si NMR study of silicate and aluminosilicate glasses: The effect of network-modifying cations. Am. Mineral., 70: 332–343.

Mysen, B.O., 1988. Structure and Properties of Silicate Melts. Elsevier, Amsterdam, 354 pp.

Mysen, B.O., 1990. Distribution of aluminum between structural units in peralkaline aluminosilicate melts in the systems Li_2O–Al_2O_3–SiO_2, Na_2O–Al_2O_3–SiO_2, and K_2O–Al_2O_3–SiO_2. Am. Mineral., 75: 120–134.

Mysen, B.O. and Boettcher, A.L., 1975. Melting of a hydrous mantle, II. Geochemistry of crystals and liquids formed by anatexis of mantle peridotite at high pressures and high temperatures as a function of controlled activities of water, hydrogen and carbon dioxide. J. Petrol., 16: 549–590.

Mysen, B.O. and Virgo, D., 1986a. Volatiles in silicate melts at high pressure and temperature, 2. Water in melts along the join $NaAlO_2$–SiO_2 and a comparison of solubility mechanisms of water and fluorine. Chem. Geol., 57: 333–358.

Mysen, B.O. and Virgo, D., 1986b. Volatiles in silicate melts at high pressure and temperature, 1. Interaction between OH groups and Si^{4+}, Al^{3+}, Ca^{2+}, Na^+ and H^+. Chem. Geol., 57: 303–331.

Mysen, B.O., Finger, L.W., Seifert, F.A. and Virgo, D., 1982. Curve-fitting of Raman spectra of amorphous materials. Am. Mineral., 67: 686–696.

Nakamoto, K., 1978. Infrared and Raman Spectra of Inorganic and Coordination Compounds. Wiley, New York, N.Y., 448 pp.

Nakamoto, K., Margoshes, M. and Rundle, R.E., 1955. Stretching frequencies as a function of distances in hydrogen bonds. J. Am. Chem. Soc., 77: 6480–6486.

Navrotsky, A., 1987. Calorimetric studies of melts, crystals and glasses, especially in hydrous systems. In: B.O. Mysen (Editor), Magmatic Processes: Physicochemical Principles. Geochem. Soc. Spec. Publ., No. 1, pp. 411–422.

Oxtoby, S. and Hamilton, D.L., 1978. The discrete association of water with Na_2O and SiO_2 in Na–Al silicate melts. Contrib. Mineral. Petrol., 66: 185–188.

Paterson, M.S., 1982. The determination of hydroxyl by infrared absorption in quartz, silicate glasses and similar materials. Bull. Minéral., 105: 20–29.

Persikov, E.S., 1974. Experimental studies of the solubility of water in granitic melts and kinetics of melt–water equilibria at high pressures. Int. Geol. Rev., 16: 1062–[illegible].

Phillips, J.C., 1982. Spectroscopic and morphological structure of tetrahedral oxide glasses. Solid State Phys., 37: 93–171.

Phillips, J.C., 1984. Microscopic origin of anomalously narrow Raman lines in network glasses. J. Non-Cryst. Solids, 63: 347–355.

Revesz, A.G. and Walrafen, G.E., 1983. Structural interpretation of some of the Raman lines from vitreous silica. J. Non-Cryst. Solids, 54: 323–355.

Satherley, K. and Smedley, S.I., 1985. The electrical conductivity of some hydrous and anhydrous molten silicates as a function of temperature and pressure. Geochim. Cosmochim. Acta, 49: 769–777.

Scholze, H., 1960. Zur Frage der Unterscheidung zwischen H_2O-Molekülen und OH-Gruppen in Gläsern und Mineralen. Naturwissenschaften, 47: 226–227.

Seifert, F.A., Mysen, B.O. and Virgo, D., 1981. Quantitative determination of proportions of anionic units in silicate melts. Carnegie Inst. Washington, Yearbk., 80: 301–302.

Seifert, F.A., Mysen, B.O. and Virgo, D., 1982. Three-dimensional network structure in the systems SiO_2–$NaAlO_2$, SiO_2–$CaAl_2O_4$ and SiO_2–$MgAl_2O_4$. Am. Mineral., 67: 696–711.

Sen, N. and Thorpe, M.F. 1977. Phonons in AX_2 glasses: From molecular to bank-like modes. Phys. Rev. Lett., B15: 4030–4038.

Sharma, S.K. and Simons, B., 1981. Raman study of crystalline polymorphs and glasses of spodumene composition quenched from various pressures. Am. Mineral., 66: 118–126.

Sharma, S.K., Mammone, J.F. and Nicol, M.F., 1981. Raman investigation of ring configurations in vitreous silica. Nature (London), 292: 140–141.

Shaw, H.R., 1963. Obsidian–H_2O viscosities at 1000 and 2000 bars in the temperature range 700° and 900°C. J. Geophys. Res., 68: 6337–6343.

Silver, L. and Stolper, E., 1989. Water in albitic glasses. J. Petrol., 30: 667–710.

Stolen, R.H. and Walrafen, G.E., 1976. Water and its relation to broken total defects in fused silica. J. Chem. Phys., 64: 2613–2631.

Stolper, E., 1982. The speciation of water in silicate melts. Geochim. Cosmochim. Acta, 46: 2609–2620.

Takata, M., Acocella, J., Tomozawa, M. and Watson, E.B., 1981. Effect of water content on the electrical conductivity of Na_2O–SiO_2 glass. J. Am. Ceram. Soc., 64: 719–724.

Uys, J.M. and King, T.B., 1963. The effect of basicity on the solubility of water in silicate melts. Trans. Am. Inst. Min. Metall. Eng., 227: 492–500.

Walrafen, G.E., 1967. Raman spectral studies of the effect of temperature on water structure. J. Chem. Phys., 44: 114–126.

Watson, E.B., 1979. The effect of dissolved water on cesium diffusion in molten granite. Eos (Trans. Am. Geophys. Union), 60: 402 (abstract).

Yamamoto, K., Nakanishi, T., Kasahara, H. and Abe, K., 1983. Raman scattering of SiF_4 molecules in amorphous fluorinated silicon. J. Non-Cryst. Solids, 59/60: 213–216.